

**CALCULATION OF DENSITIES, TEMPERATURES, CURRENTS,
FLOWS AND ELECTRIC FIELDS IN THE SCRAPE-OFF LAYER AND
DIVERTOR OF TOKAMAK PLASMAS**

W. M. Stacey
weston.stacey@nre.gatech.edu
Georgia Institute of Technology
Atlanta, GA 30332 USA
August, 2008

Abstract

A computationally tractable model for the calculation of ion and impurity densities, temperature, currents, particle flows and electric fields along the separatrix in the divertor and scrape-off layer of tokamak plasmas is described and applied to calculate the effects of particle drifts and the direction of the toroidal magnetic field on these quantities. Several experimentally observed phenomena—double reversal of the parallel ion velocity in the SOL, enhanced core penetration of argon injected into the divertor when the grad-B ion drift is into rather than away from the divertor—and other interesting phenomena, such as the structure of the parallel current flowing in the SOL and the reversal of the sign of the electrostatic potential in the SOL when the toroidal field direction is reversed, are predicted.

Preprint of paper submitted to Physics of Plasmas

I. Introduction

The physics of the plasma outside the last closed flux surface, or separatrix, in the edge of diverted tokamak plasmas is a subject of current research interest, both because of the intrinsic importance of the physics of the scrape-off layer (SOL) and divertor for heat removal and particle exhaust in tokamaks, but also because of the growing evidence of the influence of divertor and SOL physics on the physics of the edge pedestal region and hence on the performance parameters of the “core” plasma.

The diverse physical phenomena involved in the divertor and scrape-off layer¹ (SOL) make the calculation of the plasma properties in the edge of a tokamak plasma a formidable task. Early work provided a number of relatively simple “2-point” models (e.g. Refs. 1-5) that could calculate the density and temperatures at two points—just in front of the divertor target plates and in the SOL near the plasma mid-plane—and similar models (e.g. Refs. 5 and 6) for the calculation of currents flowing in the scrape-off layer into the divertor targets, subject to various simplifying assumptions that limit their general applicability. Pioneering efforts have now provided 2D fluid plasma transport and electromagnetic codes⁷⁻¹⁰ coupled with Monte Carlo calculations of recycling neutrals, and more recently gyrokinetic codes¹¹, which can calculate temperature and density distributions, plasma flows, currents and electric fields, etc. in great detail, without resort to many of the simplifying assumptions of the earlier models. Such codes have been able to reproduce many of the plasma and electromagnetic phenomena observed in experiments, but they are computationally intensive, which in practice limits their usage for routine experimental interpretation and theoretical analyses.

One purpose of this paper is to present a recently developed calculation of divertor and SOL physics of complexity and detail intermediate between the early “2-point” models and the more recent 2D fluid codes. The objectives of this model are 1) to include many of the important plasma and electromagnetic phenomena in the calculation of the densities, temperatures, flows, currents and electric fields in the SOL and divertor, while 2) achieving a calculation that is computationally tractable enough to be usable on a routine basis in the analysis of experiments, as a “boundary condition” model for core plasma transport calculations, to generate “background” plasma edge properties for neutral particle transport codes, etc.

A number of stratagems were adopted in order to obtain a computationally tractable calculation without neglecting important physical phenomena. First, the important effects of the non-uniform magnetic geometry were treated by using analytical representations of cross-field particle drifts and currents. This allows the geometry of the SOL and divertor to be represented by a simplified 2D strip geometry connecting the inner and outer divertor target plates along the magnetic field lines. Second, radial transport effects were represented analytically, enabling the actual numerical transport calculation to be carried out in one dimension along the field lines. Third, the first order differential equations resulting from particle, momentum and energy balance and the current divergence condition were solved iteratively, rather than being combined into higher order differential equations to eliminate variables. Fourth, integral particle, momentum and energy balances (i.e. something similar to the 2-point models) were used to constrain boundary conditions for the transport equations as part of the iteration procedure.

As an application of this calculation model to a problem of current interest, an analysis of the effects of curvature, grad-B and ExB drifts was performed for a model problem representative of the DIII-D¹² divertor and scrape-off layer for a H-mode discharge. The particular objective of these calculations was elucidation of the mechanisms by means of which particle drifts and the direction of the toroidal magnetic field affect the densities, temperatures, flows, currents and electric fields in the divertor and scrape-off layer.

The calculation model is described in the next section II, the calculated effects of grad-B, curvature and ExB drifts on divertor and SOL plasma parameters are discussed in the following section III, and a brief summary is provided in the final section IV.

II. Calculation Model

Geometrical model

The plasma outside the separatrix is modeled as “stack” of 2D strips, or “ribbons”, that spiral about the core plasma (q times between X-points) following the magnetic field lines from the inner to the outer divertor target plate. A poloidal projection of this geometry is shown in Fig. 1. Non-uniformities in the magnetic geometry are represented by particle “drifts” to account for the effects of field gradients and curvature while retaining a simple computational geometry.

The parameter ξ designates the distance along the field lines from the inner ($\xi = \xi_{in}$) to the outer ($\xi = \xi_{out}$) divertor targets.

Radial transport

The 2D transport problem in this strip is reduced to 1D by writing the divergence of the particle and heat fluxes as, e.g. for the particle flux $\nabla \cdot \Gamma = d\Gamma/d\xi + d\Gamma/dr$ and approximating the radial term by following experiment observation to assume that the density (and temperature) exponentially attenuate radially outward from the separatrix, $n = n_{sep} \exp(-r/\Delta_n)$ in the SOL. Requiring continuity across the separatrix of the ion particle flux Γ_{\perp}^{sep} from the core into the SOL with a diffusive radial particle flux in the SOL $\Gamma_r = -D_{\perp} dn/dr$ identifies $\Delta_n = n_{sep} D_{\perp} / \Gamma_{\perp}^{sep}$. At the outer edge of the SOL, which is taken as a distance $\varepsilon \Delta_n$ outside the separatrix, the radially outward ion flux lost from the SOL plasma is $\Gamma_{\perp}^{sol} = D_{\perp} \Delta_n^{-1} n_{sep} e^{-\varepsilon}$. This leads to an approximation $d\Gamma/dr \approx (\Gamma_{\perp}^{sol} - \Gamma_{\perp}^{sep}) / \Delta_n = -(\Gamma_{\perp}^{sep} / \Delta_n)(1 - e^{-\varepsilon}) \equiv -\Gamma_{\perp} / \Delta_n$ for the radial contribution to the divergence of the particle flux. In this work, $\varepsilon = 1$ is used in the SOL (between X-points) and $\varepsilon = 3$ is used in the divertor channels to reflect the expansion of field line separation.

In the divertor channel, the density and temperature distributions outside the separatrix are observed to first increase sharply with “radial” distance from the separatrix, peak, and then attenuate exponentially with further distance from the separatrix. This observation is indicative of a diffusive type loss both inward into the private flux region and outward towards the divertor chamber walls. There is no incident ion particle flux from the core, of course, so only the radial transport loss term $-D_{\perp} n / \Delta_n^2$ is present in the divertor.

A similar argument can be used to approximate the radial component of the divergence of the heat flux, Q . When it is further assumed that parallel heat flux is dominated by electron heat conduction, $Q \approx \kappa_{\parallel} dT/d\xi = \kappa_0 T^{5/2} dT/d\xi$, the resulting approximation of radial transport is $dQ/dr \approx -(Q_{\perp}^{sep} / \Delta_E)(1 - e^{-\varepsilon}) \equiv -Q_{\perp} / \Delta_E$, where $\Delta_E = 2\chi_{\perp} n_{sep} T_{sep} / 7Q_{\perp}^{sep}$, with Q_{\perp}^{sep} representing

the heat flux from the core flowing across the separatrix into the SOL. In the divertor channel only the transport loss term $-nT\chi_{\perp}/\Delta_E^2$ is present.

Thus, the radial transport is represented by the parameters Δ_n and Δ_E . The Bohm transport coefficients $D_{\perp} = T/16eB$, $\chi_{\perp} = 5T/32eB$ are often used, but any other transport model can equally well be used, or experimentally observed attenuation coefficients can be used.

Temperature, density and velocity distributions

The parallel energy balance equation solved for the heat flux Q in the SOL and divertor in a strip running from the inner divertor target plate around the plasma in a clockwise positive direction to the outer diver plate, as shown in Fig. 1, is

$$\begin{aligned} \frac{dQ}{d\xi} = & \frac{Q_{\perp}}{\Delta_E} - n_z n_e L_z - E_{ion} n_e n_o \langle \sigma v \rangle_{ion} + f I_{ion} n_i n_e \langle \sigma v \rangle_{rec} - \frac{3}{2} n_i n_o^c \langle \sigma v \rangle_{cxel} \\ & + j_{\parallel} E_{\parallel} \equiv \frac{Q_{\perp}}{\Delta_E} - P_{rad} - P_{at} + P_{\Omega} \end{aligned} \quad (1)$$

where Q_{\perp} is the perpendicular heat flux across the separatrix into the SOL (reduced by the radial transport heat loss), the second term represents impurity radiation (and bremsstrahlung) cooling, and the last three atomic physics terms represent ionization cooling, recombination heating, and charge-exchange plus elastic scattering cooling of the plasma. The sheath boundary conditions specify a heat flux into the inner and outer divertor plates

$$Q_{in} = -n_{in} c_{s,in} T_{in} \gamma_{in}, \quad Q_{out} = n_{out} c_{s,out} T_{out} \gamma_{out} \quad (2)$$

where

$$\gamma = \frac{2T_i}{T_e} + \frac{2}{1-\delta} + \frac{1}{2} \ln \left(\frac{(1-\delta)m_i/m_e}{2\pi(1+T_i/T_e)} \right) \quad (3)$$

is the sheath coefficient and δ is the secondary electron emission coefficient.

The parallel particle balance equation is

$$\frac{d\Gamma}{d\xi} = \frac{\Gamma_{\perp}}{\Delta_n} + n_e (n_o \langle \sigma v \rangle_{ion} - n_i \langle \sigma v \rangle_{rec}) \equiv \frac{\Gamma_{\perp}}{\Delta_n} + n_e (v_{ion} - v_{rec}) \quad (4)$$

where Γ_{\perp} is the perpendicular particle flux from the core across the separatrix into the SOL (reduced by the radial particle loss) and “ion” and “rec” refer to ionization and recombination.

The sheath boundary conditions specify that the particle fluxes into the target plates are

$$\Gamma_{in} = -n_{in} c_{s,in}, \Gamma_{out} = n_{out} c_{s,out} \quad (5)$$

where c_s is the sound speed. In both Eqs. (2) and (5), the minus sign indicates that the flux is into the plate at the inner divertor target in the negative sense of the parallel coordinate ξ . These incident ions are recycled as neutral atoms and molecules, with the latter being dissociated immediately and transported as low energy atoms until they have a charge-exchange or elastic scattering collision, upon which they are combined with the higher energy reflected neutrals and transported throughout the divertor and SOL and inward across the separatrix.

Since both the particle and heat fluxes have inward flowing boundary conditions at both the inner and outer target plates, there must be stagnation points (not necessarily the same) in the particle and heat flows somewhere in the SOL (or divertor). Integrating Eq. (1) from the stagnation heat flux point ($Q_{stag} = 0$) to either target plate and using the boundary condition of Eq. (2) and integrating Eq. (4) from the particle flux stagnation point ($\Gamma = 0$) to either target plate and using the boundary condition of Eq. (5) then yields, for each target, a pair of equations which can be solved for the temperature just in front of the target plate

$$T_{out} = \frac{\int_{\xi_{stagQ}}^{\xi_{out}} (\frac{Q_{\perp}}{\Delta_E} - P_{rad} - P_{at}) d\xi}{\gamma_{out} \int_{\xi_{stag\Gamma}}^{\xi_{out}} (\frac{\Gamma_{\perp}}{\Delta_n} + n_e (v_{ion} - v_{rec})) d\xi}, T_{in} = \frac{\int_{\xi_{stagQ}}^{\xi_{in}} (\frac{Q_{\perp}}{\Delta_E} - P_{rad} - P_{at}) d\xi}{\gamma_{in} \int_{\xi_{stag\Gamma}}^{\xi_{in}} (\frac{\Gamma_{\perp}}{\Delta_n} + n_e (v_{ion} - v_{rec})) d\xi} \quad (6)$$

and for the density just in front of the target plates

$$n_{out} = \frac{\int_{\xi_{stag}\Gamma}^{\xi_{out}} \left(\frac{\Gamma_{\perp}}{\Delta_n} + n_e (v_{ion} - v_{rec}) \right) d\xi}{\sqrt{\frac{2T_{out}}{m}}}, \quad n_{in} = \frac{\int_{\xi_{stag}\Gamma}^{\xi_{in}} \left(\frac{\Gamma_{\perp}}{\Delta_n} + n_e (v_{ion} - v_{rec}) \right) d\xi}{\sqrt{\frac{2T_{in}}{m}}} \quad (7)$$

These conditions are used in converging the iterative solution.

Solving Eqs. (1) and (2) for

$$Q(\xi) = -n_{in} c_{s,in} T_{in} \gamma_{in} + \int_{\xi_{in}}^{\xi} \left(\frac{Q_{\perp}}{\Delta_E} - P_{rad} - P_{at} \right) d\xi' \quad (8)$$

and assuming that parallel heat transport is dominated by classical electron heat conduction

$Q(\xi) \approx q(\xi) = -\kappa_0 T^{5/2} dT/d\xi = -\frac{2}{7} \kappa_0 dT^{7/2}/d\xi$ leads to a solution for the temperature distribution in terms of the heat flux calculated from Eq. (8)

$$T^{7/2}(\xi) = T_{in}^{7/2} - \frac{7}{2\kappa_0} \int_{\xi_{in}}^{\xi} Q(\xi') d\xi' = T_{in}^{7/2} - \frac{7}{2\kappa_0} \int_{\xi_{in}}^{\xi} \left[-n_{in} c_{s,in} T_{in} \gamma_{in} + \int_{\xi_{in}}^{\xi'} \left(\frac{Q_{\perp}}{\Delta_E} - P_{rad} - P_{at} \right) d\xi'' \right] d\xi' \quad (9)$$

The parallel momentum balance equation can be written, neglecting viscosity, as

$$\frac{dM}{d\xi} \equiv \frac{d}{d\xi} (2p + nmv^2) = -m(v_{cxel} + v_{ion})\Gamma \equiv -mv_{mom}\Gamma \quad (10)$$

and integrated to solve for

$$M(\xi) = M(\xi_{in}) - \int_{\xi_{in}}^{\xi} mv_{mom}(\xi')\Gamma(\xi') d\xi' = 4n_{in}T_{in} - \int_{\xi_{in}}^{\xi} mv_{mom}(\xi')\Gamma(\xi') d\xi' \quad (11)$$

$M(\xi)$ can then be equated to $(2p + nmv^2)$ to obtain a quadratic equation in $n(\xi)$

$$(2p(\xi) + n(\xi)mv^2(\xi)) \equiv (2n(\xi)T(\xi) + m\Gamma^2(\xi)/n(\xi)) = M(\xi) \quad (12)$$

which yields a solution for the plasma ion density

$$n(\xi) = \frac{M(\xi)}{4T(\xi)} \left[1 \pm \sqrt{1 - 8mT(\xi)\Gamma^2(\xi)/M^2(\xi)} \right] \quad (13)$$

that can be used in the definition of Γ to obtain the plasma flow velocity

$$v(\xi) = \Gamma(\xi)/n(\xi) \quad (14)$$

The sheath boundary condition on the parallel flow velocity is

$$v(\xi_{in}) = -c_{s,in} \equiv -\sqrt{\frac{2T_{in}}{m}}, \quad v(\xi_{out}) = c_{s,out} \equiv \sqrt{\frac{2T_{out}}{m}} \quad (15)$$

In all calculations to date, the larger value obtained using the + sign in Eq. (13) has been of the magnitude observed in experiment, but the smaller value has not been physically unreasonable, perhaps implying the existence of a lower density divertor regime.

Equation (10) can be integrated from the inner divertor target plate to the outer divertor target plate to obtain

$$4n_{out}T_{out} - 4n_{in}T_{in} = - \int_{\xi_{in}}^{\xi_{out}} m\Gamma(\xi)v_{mom}(\xi) d\xi \quad (16)$$

demonstrating that a difference in pressure at the two divertor plates requires momentum dissipation (by atomic physics processes in this development) in the plasma flow between the two target plates. Equation (10) can also be integrated from the flow stagnation point to either

divertor plate to obtain a relation between for the pressure at the stagnation point and the pressure in front of the divertor target plate

$$(nT)_{stag\Gamma} = 2n_{in}T_{in} + \frac{1}{2} \int_{\xi_{stag\Gamma}}^{\xi_{in}} m\Gamma(\xi)v_{mom}(\xi)d\xi = 2n_{out}T_{out} + \frac{1}{2} \int_{\xi_{stag\Gamma}}^{\xi_{out}} m\Gamma(\xi)v_{mom}(\xi)d\xi \quad (17)$$

The well-known “2-point” SOL-divertor model consists of the set of Eqs. (6) and (7) for the temperature and the density at the divertor target plus Eqs. (9) evaluated at the flow stagnation point and Eq.(17) for the temperature and density at the flow stagnation point.

Electrostatic potential

The electrostatic potential satisfies the electron parallel momentum balance equation

$$\frac{d\phi}{d\xi} = \frac{0.71}{e} \frac{dT}{d\xi} + \frac{1}{ne} \frac{dp}{d\xi} - \frac{j_{\parallel}}{\sigma_{\parallel}} \quad (18)$$

which can be integrated to obtain

$$\phi(\xi) = \phi_{in} + \frac{1.71}{e} [T(\xi) - T_{in}] + \int_{\xi_{in}}^{\xi} \frac{T(\xi')}{en(\xi')} \frac{dn(\xi')}{d\xi'} d\xi' - \int_{\xi_{in}}^{\xi} \frac{j_{\parallel}(\xi')}{\sigma_{\parallel}(\xi')} d\xi' \quad (19)$$

where the potential just in front of the target plate is given by the current-potential sheath relation between the potential just in front of the plate ($\phi_{in,out}$) and the current ($j_{pl}^{in,out}$) into the plate

$$\phi_{in} = -\frac{T_{in}}{e} \ln \left[\frac{\sqrt{m_i/\pi m_e} (1-\delta)}{1 - j_{pl}^{in}/n_{in} e c_{si,in}} \right], \quad \phi_{out} = -\frac{T_{out}}{e} \ln \left[\frac{\sqrt{m_i/\pi m_e} (1-\delta)}{1 - j_{pl}^{out}/n_{out} e c_{si,out}} \right] \quad (20)$$

where $\sigma_{\parallel} = 2n_e e^2 \tau_e / m_e$, $\tau_e = 3\sqrt{m_e} T^{3/2} / 4\sqrt{2\pi} n_e \ln \Lambda e^4$.

Parallel current

The net current density into the target plates is given by the sum of the ion current density $ne c_{si}$ and the electron current density, $\frac{1}{4}n(-e)\bar{c}_e e^{e\phi/T}$ for a Maxwellian distribution,

$$j_{pl}^{in} = ne \left[c_{si} - \frac{1}{4} \bar{c}_e e^{e\phi/T_e} \right] \quad (21)$$

where $\bar{c}_e = (8T_e/\pi m_e)^{1/2}$ is the average electron speed for a Maxwellian distribution.

The current density must be divergence-free

$$\nabla \cdot \mathbf{j} \equiv \frac{dj_{\parallel}}{d\xi} + \frac{dj_{\perp}}{d\ell_{\perp}} + \frac{dj_r}{dr} = 0 \quad (22)$$

which may be solved for

$$j_{\parallel}(\xi) = -j_{pl}^{in} - \int_{\xi_{in}}^{\xi} \left[\frac{dj_{\perp}}{d\ell_{\perp}} + \frac{dj_r}{dr} \right] d\xi', \quad (23)$$

The minus sign in front of the first term on the right results from the fact that Eq.(21) specifies the current into the inner divertor plate, while the positive sense of the current in this model is out of the inner divertor plate (but into the outer divertor plate); i.e. $j_{\parallel}(\xi_{in}) = -j_{pl}^{in}$.

These cross-field currents are driven by gradB and curvature drifts, as discussed in the following section. They are not driven by ExB drifts, which are the same for ions and electrons and hence do not produce currents, nor by diamagnetic currents which are almost divergence-free. Cross-field currents also may be driven by cross-field transport, viscosity and other mechanisms that have different effects on ions and electrons, but these mechanisms have been found^{9,10} to be smaller and are not considered at present.

Grad-B and curvature drifts

The grad-B and curvature drifts are

$$\begin{aligned} v_{\nabla B} &= \frac{T}{e} \frac{\mathbf{B} \times \nabla B}{B^3} \approx \frac{T}{eRB} \mathbf{n}_z, \quad v_c = -\frac{mv_{\parallel}^2}{e} \frac{\mathbf{B} \times \mathbf{R}}{B^2 R^2} \approx \frac{mv_{\parallel}^2}{eRB} \mathbf{n}_z, \\ v_B &\equiv v_{\nabla B} + v_c \approx \frac{3T}{eRB} \mathbf{n}_z \end{aligned} \quad (24)$$

where \mathbf{n}_z is a unit vector in the vertical direction, up or down depending on the direction of \mathbf{B} , and $v_{\parallel} \approx v_{th}$. The drifts are in opposite directions for ions and electrons because of the charge sign difference, producing a current

$$\mathbf{j}_B = 2nev_B \approx \frac{6nT}{BR} \mathbf{n}_z \quad (25)$$

At this point, a specific current and magnetic field configuration is adopted, as shown in Figs. 1-4. For this configuration, the vertical unit vector \mathbf{n}_z is directed downward. Thus, the radial drift currents are radially inward from the SOL into the core in the upper hemisphere ($0 \leq \theta \leq \pi$) and radially outward from the core into the SOL in the lower hemisphere ($\pi \leq \theta \leq 2\pi$), as indicated in Fig. 2.

The ion grad-B and curvature drifts also produce a parallel particle drift

$$\Gamma_{\nabla B}^{\parallel} = (\mathbf{n}_{\parallel} \cdot \mathbf{n}_z) \Gamma_{\nabla B}^z = \left(\frac{B_{\theta}}{B} \cos \theta \right) \frac{3nT}{eBR} \quad (26)$$

which is downward in both the inner and outer SOLs and divertors, as indicated in Fig. 2. Here, the angle θ is with respect to the outboard mid-plane. In the divertor, $\cos \theta$ is replaced by $\sin \alpha$, where α is the angle of incidence with respect to the horizontal of the separatrix, as illustrated in Fig. 2.

Using Eq. (25) to evaluate the radial drift current in Eq. (23) and adding the poloidal drift current from Eq. (26) provides an equation for the resulting parallel current in the SOL as a result of the divergence of the radial grad-B and curvature drift currents plus the parallel drift current

$$j_{\parallel}(\xi) = j_{\parallel}(\xi_{in}) + \int_{\xi_{in}}^{\xi} \left[\frac{6n(\xi')T(\xi')[\Delta_n^{-1} + \Delta_T^{-1}]}{RB} (\mathbf{n}_r \cdot \mathbf{n}_z) \right] d\xi' + 2e\Gamma_{\nabla B}^{\parallel} \equiv j_{\parallel}(\xi_{in}) + \Delta j_{\nabla B}(\xi) \quad (27)$$

The radial gradient scale lengths of temperature and density are defined in terms of the radial transport coefficients in the SOL $\Delta_n = n_{sep} D_{\perp} / \Gamma_{\perp}^{sep}$, $\Delta_T = n_{sep} T_{sep} \chi_{\perp} / Q_{\perp}^{sep}$, or they may be taken from experiment.

Solution for currents and potentials at target plates

Once the densities and temperatures are determined at the inner and outer divertor target plates (by solving Eqs. (1)-(17) in an iterative loop), Eqs.(19)-(27) can be solved for the electrostatic potentials and currents at the target plates. The current at the outer target can be evaluated from Eq. (27). Note that the integral of all the radial currents flowing from the core into the SOL plus all the radial currents flowing from the SOL into the core must vanish to maintain a neutral core plasma. The radial currents due to grad-B and curvature drifts are represented by the second term in Eq. (27), which will not vanish in general; i.e. other radial currents are needed. It is intended to include other radial currents in a future version of this model, but for now an ‘ambipolarity’ condition is imposed by adding or subtracting a constant to the term in square brackets in Eq. (27) that will cause the integral to vanish, in order to represent these other radial currents (which in effect represents the other radial currents as being distributed uniformly over the SOL). This ‘ambipolarity-constrained’ current integral is represented by $\Delta \hat{j}_{\nabla B}(\xi)$. With this representation, Eq. (27) yields a relation between the currents into the plates at the inner and outer divertor targets

$$j_{pl}^{out} \equiv j_{\parallel}(\xi_{out}) = j_{\parallel}(\xi_{in}) + 2ne\Gamma_{\nabla B}^{\parallel}(\xi_{out}) = -j_{pl}^{in} + 2ne\Gamma_{\nabla B}^{\parallel}(\xi_{out}) \quad (28)$$

Equation (19) yields a relation between the potential just in front of the inner and outer plates

$$\phi_{out} = \phi_{in} + \frac{1.71}{e} [T_{out} - T_{in}] + \int_{\xi_{in}}^{\xi_{out}} \frac{T(\xi')}{en(\xi')} \frac{dn(\xi')}{d\xi'} d\xi' - \int_{\xi_{in}}^{\xi_{out}} \frac{[j_{\parallel}(\xi_{in}) + \Delta \hat{j}_{\nabla B}(\xi')]}{\sigma_{\parallel}(\xi')} d\xi' \quad (29)$$

Using Eqs. (20) with $j_{pl}^{in} = -j_{\parallel}(\xi_{in})$ and j_{pl}^{out} given by Eq. (28) in Eq. (29) yields an equation that determines $j_{\parallel}(\xi_{in})$. Note that although the integral of the radial currents over the SOL must vanish, the current integral in Eq. (29) is weighted by $1/\sigma_{\parallel} \sim 1/T^{3/2}$ and extends also over the divertor plasmas. This equation displays the well known result that the current in the SOL is driven by differences in potentials and temperatures at the target plates and by drifts due to the non-uniformity and curvature of the magnetic field (and other causes).

The above development has implicitly assumed that the target plates are at zero potential. If the plates are biased with respect to ground, then $\phi_{in,out} \Rightarrow \phi_{in,out} + \phi_{in,out}^{bias}$ in the above equations.

ExB drifts

Although ExB drifts do not produce currents, they do produce particle flows. The parallel variation of the electrostatic potential produces a parallel electric field and a corresponding radial ExB drift.

$$E_{\parallel} = -\left(\frac{d\phi}{d\xi}\right), \quad v_{E_{\parallel} \times B}^r = \frac{\mathbf{E}_{\parallel} \times \mathbf{B}}{B^2} = \frac{-\frac{d\phi}{d\xi}}{B} \quad (30)$$

directed as illustrated in Fig. 3 for the case in which the potential is negative in front of both target plates and increases to a maximum positive value at some point towards the top of the plasma in this model.

The “radial” ExB flows from the outboard divertor channel into the private flux region and from the private flux region into the inboard divertor channel will transfer ions from the outboard divertor channel across the private flux region beneath the plasma to the inboard divertor channel¹³ .

The “radial drift” loss or gain of ions from both the SOL and the divertor channels can be represented by an ExB loss frequency

$$\nu_{E_{\parallel}xB}(\xi) = \frac{v_{E_{\parallel}xB}^r(\xi)}{\varepsilon \Delta_n} \quad (31)$$

where Δ_n is an estimate of the “radial width” of the SOL calculated as discussed for Eq. (6) and $\varepsilon \approx 3$ is a flux surface expansion factor taking into account the widening of the SOL into the divertor channel. Assuming that some fraction f_{ExB} of the ions lost into the private flux region from the outboard divertor channel flow into the inboard divertor channel, the source density of ions to the inboard divertor channel may be represented

$$S_{E_{\parallel}xB}^{in} = \frac{f_{ExB} \int_{\xi_{out}}^{\xi_{Xout}} \nu_{E_{\parallel}xB}(\xi) n(\xi) d\xi}{\int_{\xi_{in}}^{\xi_{Xin}} d\xi} \quad (32)$$

where $\xi_{Xout,in}$ denotes the location of the X-point in the outer SOL-divertor.

The particle balance Eq. (4) in the divertor channels now becomes

$$\frac{d\Gamma}{d\xi} = \frac{\Gamma_{\perp}}{\Delta_n} + n_e (v_{ion} - v_{rec}) + n_i (v_{E_{\parallel}xB} + v_B) + S_{E_{\parallel}xB}^{in} \quad (33)$$

where the source term $S_{E_{\parallel}xB}^{in}$ is only present in the inboard divertor channel, for the field configuration shown in Figs. 1-4. The quantity v_B is a radial transport frequency defined by an

expression like Eq. (29) but using the radial curvature and grad-B drifts given by Eq. (24). Positive radial drifts correspond to outward ion flow from the core into the SOL and constitute a source of ions to the SOL, while negative radial flows correspond to inward flows of ions from the SOL into the core and constitute a loss of ions in the SOL. In the divertor channels radial drifts in either direction constitute a loss of ions, and the radial drift frequencies in Eq. (33) are negative.

There is a radially outward directed electric field in the SOL produced by the radial temperature gradient in the SOL

$$E_r(\xi) = \frac{-d\phi}{dr} = -\phi \left(\frac{1}{\phi} \frac{d\phi}{dr} \right) \approx -\phi \left(\frac{1}{T} \frac{dT}{dr} \right) \equiv \phi \Delta_T^{-1} \quad (34)$$

which produces poloidal clockwise ExB drifts and particle fluxes in the SOL

$$v_{E_r, xB}^\theta(\xi) = \frac{\phi(\xi) \Delta_T^{-1}}{B}, \quad \Gamma_{E_r, xB}^\theta(\xi) = \frac{n(\xi) \phi(\xi) \Delta_T^{-1}}{B} \quad (35)$$

as illustrated in Fig. 4.

The component of this poloidal particle flux parallel to the field in the SOL constitutes a parallel drift particle flux

$$\Gamma_{E_r, xB}^\parallel(\xi) = \frac{B_\theta}{B} \Gamma_{E_r, xB}^\theta(\xi) = \frac{n(\xi) \phi(\xi) \Delta_T^{-1} B_\theta}{B^2} \quad (36)$$

which circulates clockwise around the SOL, as illustrated in Fig. 4.

The temperature distribution at the divertor target plate has been observed to peak somewhat outside the separatrix (i.e. to the right/left of the separatrix in the outer/inner divertor), causing the direction of the radial electric field along the separatrix to change from outward in the SOL to inward into the private flux region in the divertor channel. This produces a parallel drift particle flux downward in the inner divertor and upward in the outer divertor, as illustrated in Fig. 4.

Both the parallel particle drift fluxes [Eqs. (27) and (34)] are additive to the particle flux due to particle sources calculated from Eq. (.31).

Diamagnetic drifts

The leading order local force balance on the plasma balances the pressure gradient with a $V \times B$ force, with the result that pressure gradients drive drift velocities orthogonal both to the field and the pressure gradient. In particular, a radial diamagnetic flow is driven by the pressure gradient in the direction perpendicular to the 2D strip in which the transport calculation of this paper is being carried out

$$v_{dia}^r = \frac{-1}{neB} \frac{\partial p}{\partial \ell_{\perp}} \simeq \frac{-1}{neB} \frac{\partial p}{\partial \ell_{\theta}} \simeq \frac{-1}{neB} \frac{B}{B_{\theta}} \frac{\partial p}{\partial \xi} \quad (37)$$

The radial pressure gradient also drives a diamagnetic drift velocity in the direction perpendicular to the 2D strip along the field lines of this calculation, but this drift is not considered in this calculation.

The radial diamagnetic drift of particles out of the core is treated as a particle source, and the inward drift is treated as a particle sink, in the continuity equation, in the same manner as discussed for the gradB and $E \times B$ drifts. However, the diamagnetic drift contribution to the plasma current is divergence-free except for small terms associated with the field non-uniformity, which effect has been represented by the gradB current contribution, so the diamagnetic drift does not contribute to the parallel current in this calculation.

Total parallel ion flux

The total parallel ion flux is calculated by integrating the particle balance Eq. (33), including the radial transport and radial drift losses and sources, and adding the parallel grad-B and $E \times B$ drift fluxes of Eqs. (26) and (36)

$$\Gamma(\xi) = \Gamma_{in} + \int_{\xi_{in}}^{\xi} \left[\frac{\Gamma_{\perp}^{sep}}{\Delta_n} - \frac{D_{\perp} n}{\Delta_n^2} + n_e (v_{ion} - v_{rec}) + n_i (v_{E_{\parallel}xB} + v_B + v_{dia}) + S_{E_{\parallel}xB}^{in} \right] d\xi' \quad (38)$$

$$+ \Gamma_{\nabla B}^{\parallel}(\xi) + \Gamma_{E_r \times B}^{\parallel}(\xi)$$

with Γ_{in} given by the sheath boundary condition of Eq. (5) at the inner divertor target.

The integral balance Eqs. (7) are replaced by the following expressions for the densities just in front of the target plates

$$n_{out} = \frac{\int_{\xi_{stag}\Gamma}^{\xi_{out}} \left[\frac{\Gamma_{\perp}^{sep}}{\Delta_n} - \frac{D_{\perp} n}{\Delta_n^2} + n_e (v_{ion} - v_{rec}) + n_i (v_{E_{\parallel}xB} + v_B + v_{dia}) + S_{E_{\parallel}xB}^{in} \right] d\xi}{\sqrt{\frac{2T_{out}}{m}}}, \quad (39)$$

$$n_{in} = \frac{\int_{\xi_{stag}\Gamma}^{\xi_{in}} \left[\frac{\Gamma_{\perp}^{sep}}{\Delta_n} - \frac{D_{\perp} n}{\Delta_n^2} + n_e (v_{ion} - v_{rec}) + n_i (v_{E_{\parallel}xB} + v_B + v_{dia}) + S_{E_{\parallel}xB}^{in} \right] d\xi}{\sqrt{\frac{2T_{in}}{m}}}$$

where, as before, the source term $S_{E_{\parallel}xB}^{in}$ only obtains in the inner divertor for the magnetic field geometry of Figs 1-4.

Viscosity

Inclusion of parallel viscosity introduces a term

$$-\frac{d\pi}{d\xi} = \frac{d}{d\xi} \left(\eta \frac{dv}{d\xi} \right) = \frac{d}{d\xi} \left[\eta \left(v_{ion} - v_{rec} + \frac{\Gamma_{\perp}}{n\Delta_n} - \frac{\Gamma}{n} \left(\frac{1}{n} \frac{dn}{d\xi} \right) \right) \right] \quad (40)$$

on the right side of Eq. (12). This changes the solution for $M(\xi)$ of Eq. (13) to

$$M(\xi) = 4n_{in}T_{in} - \int_{\xi_{in}}^{\xi} m v_{mom}(\xi') \Gamma(\xi') d\xi' + \left[\eta \left(v_{ion} - v_{rec} + \frac{\Gamma_{\perp}}{n\Delta_n} - \frac{\Gamma}{n} \left(\frac{1}{n} \frac{dn}{d\xi} \right) \right) \right]_{\xi_{in}}^{\xi} \quad (41)$$

The Braginskii parallel viscosity coefficient $\eta = 1.96nT\tau_i$, $\tau_i = 3\sqrt{m_i}T^{3/2}/4\sqrt{\pi}n\ln\Lambda e^4$ is used.

Inclusion of cross-field viscous terms introduces additional cross-field currents, which would alter the parallel current calculated from Eq. (23). The usual practice is to attribute cross field viscosity to anomalous processes represented by essentially a fitting parameter, but such terms are not included in the present model.

Neutral particle recycling

Neutral particle recycling and gas fueling effects on the SOL and divertor plasma are calculated with a simplified geometry 2D interface-current-balance model¹⁴. The atomic physics data used in the calculation are given in Refs. 15.

Impurities

The momentum balance equation (neglecting viscosity) for each individual impurity ion species, k, in a multispecies plasma can be written

$$\frac{d}{d\xi}(p_k + n_k m_k v_k^2) = z_k e n_k E_{\parallel} + R_{ke} + R_{ki} \quad (42)$$

where “e” refers to electrons and “i” refers to the main plasma ion species. A similar equation obtains for the main ion species, with “k” and “i” interchanged and the atomic physics momentum loss term $-n_i m_i (v_{el,i} + v_{cx,i})v_i$ added to the right side. The momentum balance equation for the electrons (neglecting inertia and viscosity) is

$$\frac{d}{d\xi}(p_e) = -en_e E_{\parallel} + R_{ei} + \sum_k R_{ek} \quad (43)$$

The collisional friction terms which appear in these equations are¹⁶

$$R_{ke} = \frac{n_k z_k^2}{n_i} R_{ie} = \frac{n_k z_k^2}{n_i} \left[\frac{-\eta_{\parallel} n_i e}{z_{eff}} j_{\parallel} + c_e^{(2)} \frac{n_i}{z_{eff}} \frac{dT}{d\xi} \right] \quad (44)$$

where

$$\eta_{\parallel} = \left[\frac{0.457}{1.077 + z_{eff}} + 0.29 z_{eff} \right] 2\sigma_{\parallel}^{-1}, \quad c_e^{(2)} = 1.5 \left(1 - \frac{0.6934}{1.3167 z_{eff}} \right) \quad (45)$$

and

$$R_{ki} = c_i^{(1)} n_i m_i v_{ik} (v_i - v_k) + c_i^{(2)} \frac{n_i}{z_{eff}} \frac{dT}{d\xi} \quad (46)$$

where

$$v_{ik} = \frac{m_i + m_k}{m_k} \frac{4\sqrt{2\pi} \ln \Lambda e^4 z_k^2 z_i^2 n_k}{3\sqrt{m_i} T^{3/2}}, \quad c_i^{(1)} = \frac{(1 + 0.24z_0)(1 + 0.93z_0)}{(1 + 2.65z_0)(1 + 0.285z_0)}, \quad z_0 = \frac{\sum_k n_k z_k^2}{n_i} \quad (47)$$

$$c_i^{(2)} = \frac{1.56(1 + \sqrt{2}z_0)(1 + 0.52z_0)}{(1 + 2.65z_0)(1 + 0.285z_0)} \frac{1}{z_0 + \sqrt{(1 + m_i/m_k)/2}}$$

A particle continuity equation obtains for each ion species

$$\frac{d\Gamma_k}{d\xi} = S_k - \frac{D_{\perp k} n_k}{\Delta_n^2} + n_k (v_{E_{\parallel} \times B, k} + v_{B, k} + v_{dia, k}) + S_{E_{\parallel} \times B, k}^{in} \quad (48)$$

where the second term on the right represents transport loss perpendicular to the field lines and the first term represents the source of impurity particles, and the last two terms on the right represent the radial drifts of ions between the SOL and the core and the $E_{\parallel} \times B$ drifting of impurities from the outer to the inner divertor channel (in the geometry of this paper).. For injected impurities, this source is just the local injection rate. For intrinsic impurities (e.g. carbon) this source density is $S_k = \Gamma_{div, i} Y_{ik} / L_k$, where $\Gamma_{div, i}$ is the incident main ion flux on the divertor target plate, Y_{ik} is the sputtering yield for target material “k” for ions of species “i”

(calculated from Ref. 17), and L_k is the distance along the field lines in front of the target plate over which the sputtered atoms become ionized (a few cm).

The boundary conditions for the impurity ions are the sheath boundary condition on impurity ion velocity into the target plate at the sound velocity, $v_k = c_{sk} = \sqrt{2T/m_k}$, and the integral particle balance condition of the particle flux incident on the divertor targets

$$\begin{aligned}\Gamma_{in,k} &= -(1-R_k^{in})n_{k,in}v_{k,in} = -(1-R_k^{in}) \int_{\xi_{in}}^{\xi_{stag}\Gamma} \left(S_k - \frac{D_{\perp k} n_k}{\Delta_n^2} + n_k (v_{E_{\parallel} \times B, k} + v_{B, k} + v_{dia, k}) + S_{E_{\parallel} \times B, k}^{in} \right) d\xi, \\ \Gamma_{out,k} &= (1-R_k^{out})n_{k,out}v_{k,out} = (1-R_k^{out}) \int_{\xi_{out}}^{\xi_{stag}\Gamma} \left(S_k - \frac{D_{\perp k} n_k}{\Delta_n^2} + n_k (v_{E_{\parallel} \times B, k} + v_{B, k} + v_{dia, k}) + S_{E_{\parallel} \times B, k}^{in} \right) d\xi\end{aligned}\quad (49)$$

The incident impurity ions are assumed to be recycled with reflection coefficient R_k as a return flux of impurity ions (i.e. ionization is assumed to take place immediately).

The total parallel impurity particle flux is obtained by integrating Eq. (45) and adding the grad-B and $E_{\parallel} \times B$ drift particle fluxes calculated as discussed above for the main ions but taking into account the difference in mass and charge.

$$\Gamma_k(\xi) = \Gamma_{k,in} + \int_{\xi_{in}}^{\xi} \left(S_k - \frac{D_{\perp k} n_k}{\Delta_n^2} + n_k (v_{E_{\parallel} \times B, k} + v_{B, k} + v_{dia, k}) + S_{E_{\parallel} \times B, k}^{in} \right) d\xi + \Gamma_{\nabla B, k}^{\parallel}(\xi) + \Gamma_{E_{\parallel} \times B, k}^{\parallel}(\xi) \quad (50)$$

The momentum balance Eq. (42) can be integrated to obtain an equation for the impurity density distribution

$$\begin{aligned}n_k(\xi)T(\xi) + m_k v_k(\xi) \Gamma_k(\xi) &= n_{in,k} T_{in} + m_k v_{in,k} \Gamma_{in,k} + \\ \int_{\xi_{in}}^{\xi} n_k(\xi') &\left[-z_k e \frac{d\phi}{d\xi} + z_k^2 \left(\frac{c_e^{(2)}}{z_{eff}} + c_i^{(2)} \right) \frac{dT}{d\xi} - \frac{z_k^2 \eta_{\parallel} e}{z_{eff}} j_{\parallel} + c_i^{(1)} m_k v_{ki} \left(\frac{\Gamma_i}{n_i} - \frac{\Gamma_k}{n_k} \right) \right] d\xi',\end{aligned}\quad (51)$$

Integrating the electron momentum balance of Eq. (43) yields an expression for the electrostatic potential that now explicitly accounts for impurities

$$\phi(\xi) = \phi_{in} + \frac{[1 + c_e^{(2)} \beta / z_{eff}]}{e} [T(\xi) - T_{in}] + \int_{\xi_{in}}^{\xi} \frac{T(\xi')}{en(\xi')} \frac{dn(\xi')}{d\xi'} d\xi' - \int_{\xi_{in}}^{\xi} \frac{\beta \eta_{\parallel}}{z_{eff}} j_{\parallel}(\xi') d\xi' \quad (52)$$

where $\beta = 1 + \sum_k n_k z_k^2 / n_i / 1 + \sum_k n_k z_k / n_i$, and ϕ_{in} is given by the sheath relation of Eq. (20).

Solution procedure

The coupled set of nonlinear equations described above are solved numerically, using iterative procedures, the convergence of which is a somewhat delicate process. This solution procedure is incorporated in an integrated modeling code⁴ which solves the core plasma power and particle balances to calculate the particle and heat fluxes $(\Gamma_{\perp}^{sep}, Q_{\perp}^{sep})$ flowing across the separatrix from the core into the SOL, the 2-point equations for the divertor and SOL which provides the background plasma parameters for the neutral calculation, and the 2D transport of recycling neutrals. This calculation also provides starting conditions for the iterative solution.

III. Effects of drifts on the divertor-SOL plasma distributions

As discussed above and as illustrated previously in a conglomerate way by calculations with the 2D fluid edge codes UEDGE^{9,18} and SOLIPS¹⁰, particle drifts due to magnetic field gradients and curvature, electric fields, and pressure gradients have a major impact on determining the distribution of ion densities, temperature, ion flows, currents, electric fields, etc. in the divertor and scrape-off layer of tokamaks. The calculation of the previous section provides an excellent means for isolating and elucidating these effects, to which purpose a series of model problem calculations have been performed.

In order to insure a realistic plasma edge regime, the model problem had machine and plasma core parameters of a DIII-D H-mode discharge, with two exceptions. The two divertor legs were symmetrized (i.e. made more like the figures above than the more asymmetric divertor

configuration actually found in DIII-D) in order to avoid geometrical asymmetries that would otherwise additionally complicate the interpretation of the results of the calculations. In such a model problem, the solution in the absence of drifts should be symmetric. Secondly, the D-shape of the plasma was not retained in modeling the essentially vertical grad-B and curvature drifts, with the effect of making the radial and poloidal (parallel) components of these drifts of symmetric magnitude in the inner and outer SOL.

The model ($R = 1.7$ m, $a = 0.6$ m, $\kappa = 1.8$, $B = 2.0$ T, $I = 1.2$ MA, $q_{95} = 4$) represented a lower single null divertor plasma with the toroidal field such that the grad-B ion drift was down into the divertor; i.e. the configuration illustrated in Figures 1-4. Another calculation was made in which the toroidal magnetic field direction was reversed. The power and particle fluxes into the SOL from the core plasma were calculated to match experimental conditions for an H-mode discharge.

The equations of the previous section were numerically integrated over a grid structure along the field lines from the inner to the outer divertor plates. A small (5 cm in the parallel dimension, about 1 cm in the poloidal dimension normal to the target plates) recycling region in front of each divertor plate, a pre-recycling region of twice that length, and 8 other regions represented each divertor channel up to and including the X-point region (total length of each 2.95 m along field lines). The SOL plasma from inner to outer X-points (parallel distance 53.02 m) was divided into 30 equal regions. With reference to Fig. 1, the recycling regions are 1 and 50, the inner and outer X-points are in regions 10 and 41, the inner and outer mid-planes are in regions 18 and 33, and the “crown” at the top is regions 25 and 26. The symmetry point is between regions 25 and 26. All results will be plotted against region number. With the numerical integration scheme employed in this paper, the densities, temperature and quantities constructed from them, such as the grad-B drift velocities, were calculated as average values over each region (e.g. the density shown in the following figures for location “1” is an average density over the first, recycling region in front of the inner divertor, and the density shown for location “33” is an average over the region containing the outer SOL mid-plane). However, quantities such as the parallel particle fluxes and particle velocities, parallel currents, electrostatic potential and associated electric fields and ExB drift velocities were calculated at the interfaces between regions (e.g. the currents and velocities shown for location “1” are the values at the inner divertor target plate, the currents and velocities shown for location “26” are the

values at the symmetry point between regions 25 and 26, and the currents and velocities shown for location “51” are the values at the outer divertor plate.

Particle sources were treated as follows. The gas fueling source for the deuterium (1.5×10^{20} #/s into the upper outboard plasma chamber) was represented explicitly, and the resulting neutral atoms were transported through the edge region across the separatrix to fuel the core plasma. An average ion flux of $\Gamma_{\perp} = 1.6 \times 10^{20}$ #/m²s from the core plasma into the SOL was calculated, taking into account this neutral influx into this core, but consisting mostly of ions produced by the neutral beam particle source. The deuterium ions striking the target plates (consisting both of ions crossing the separatrix from the core and ions produced by ionization of neutral atoms in the SOL and divertor) were reflected as neutral atoms at about one-half their incident energy or re-emitted as molecules which were dissociated into 2 eV atoms in the recycling regions 1 and 50 and were then transported throughout the edge region until ionized in the divertor, SOL or plasma edge inside the separatrix.

Two impurity ion species were modeled, carbon which is an intrinsic impurity, and argon which is sometimes used to enhance radiation. The carbon source was the calculated sputtering of the deuterium ions incident on the divertor target plates¹⁷ and was distributed over the first two regions (i.e. 1 and 2, 49 and 50) in front of the target. Carbon was transported as a single ion species with an average charge state that varied with local electron temperature along the field lines. Carbon ions returning to the target plates were reflected with a coefficient $R = 0.99$, which included in an approximate manner also the effects of carbon self-sputtering. An argon source of 2×10^{19} #/s injected in the private flux region was assumed to be pumped by the divertor plasma and was represented as a uniformly distributed particle source in the two divertor plasmas (regions 1-9 and 42-50). The argon ions incident on the divertor targets were reflected with coefficient $R=0.99$.

An average heat flux of $Q_{\perp} = 8.8 \times 10^4$ W/m² into the SOL from the core plasma was calculated from a core power balance, taking into account the 4.9 MW neutral beam heating, the small ohmic heating and the radiation from inside the separatrix. Both this heat flux and the above ion flux into the SOL from the core were uniformly distributed over the SOL regions 11-40.

Radial transport was represented by a gradient scale length of 2 cm for density and temperature.

Drifts

The radial and parallel gradB, ExB and diamagnetic drifts for the deuterium ions calculated for the magnetic configuration of Figs. 1-4, with toroidal magnetic field in the opposite direction to the plasma current, are shown in Figs. 5 and 6. The total parallel particle flux, taking into account these drifts as well as the ion flux into the SOL from the core, is also shown in Fig. 6. The diamagnetic drifts are very large just in front of the divertor plates where the parallel pressure gradients are large, but otherwise the gradB drifts are the most important.

Three different situations were calculated for the sake of comparison: i) with the grad-B, ExB and diamagnetic drifts turned off, ii) with these drifts turned on and the toroidal magnetic field in the direction opposite to the plasma current shown in Figs. 1-4, denoted B(-), and iii) with the drifts turned on and the toroidal magnetic field reversed and aligned with the current opposite to the direction shown in Figs. 1-4, denoted B(+). The drifts for case ii) are shown in Figs. 5 and 6, and the drifts for case iii) are just the negative of these. For the B(-) field direction the grad-B and curvature drifts were downward into the divertor, while for the B(+) field direction these drifts were upward away from the divertor.

Density and temperature distributions

The calculated densities and temperatures are shown in Figs. 7 and 8, respectively. The drifts do not have much effect on the deuterium density and temperature distributions, except in the recycling regions 1 and 50, where the diamagnetic and ExB drifts are large. The ExB drifts of Eq. (30) are largest near the divertor target plates because the electrostatic potential increases most rapidly there, and the diamagnetic drifts are also largest near the divertor target plates, but because the parallel pressure gradients are largest there. The effect of drifts on the carbon and argon density profiles is greater than on the deuterium density profile.

With respect to Eqs. (12) and (13), the density profile is determined by the force balance requirement that the pressure plus inertial forces are constant over the SOL and divertor except for the momentum dissipation, which takes place for the deuterium ions primarily via atomic physics collisions with neutrals in the divertor. For the parameters of this calculation, for which

the pressure in the SOL is almost 1000 Pa, the pressure term dominates the force balance, and the drift effects, which enter the density calculation via the inertial term in the force balance, have minimal effect except in the divertor, particularly in the recycling regions. The effect of drifts on the temperature profile is via the density profile and is correspondingly small in this problem, again except in the recycling regions. A greater sensitivity to drifts was found in a similar comparison¹⁰ for which the pressure was an order of magnitude lower in the SOL; such a sensitivity would result in this calculation also if the pressure contribution to the M term in Eq. (13) was decreased by an order of magnitude.

Electrical current density, potential, and fields

The grad-B and curvature drifts produce radial currents proportional to the grad-B and curvature drifts given by Eqs. (24) and indicated in Fig. 2. Without drifts, the temperature distribution was symmetric and there was no thermoelectric current. With the B(-) drifts, there was a temperature asymmetry that drove a thermoelectric current and large radial gradB drift currents that drove parallel currents in order to maintain a divergence-free total current density. This can be clearly seen by comparing Fig. 5 for the grad-B drifts to the currents calculated from Eq. (27) and shown in Fig. 9. These radial grad-B currents and the compensating parallel currents were in opposite directions for the B(-) and B(+) field directions. Note that the grad-B currents integrated to zero over the SOL to maintain ambipolarity, as discussed in connection with Eq. (27). Scrape-off layer currents of comparable magnitude have been measured in DIII-D H-mode discharges¹⁹, but we are unaware of any measurements of current profiles in the SOL.

With the drifts turned off, the symmetric temperature and density distributions shown in Figs. 8 and 7 produced the symmetric electrostatic potential distribution shown in Fig. 10, as calculated from Eq. (19) using Eqs. (20), (28) and (29). Turning on the grad-B drift and changing the direction of the toroidal magnetic field both produce a dramatic change in the parallel distribution of the electrostatic potential, primarily because to the differences in the parallel currents shown in Fig. 9.

Differentiation of the electrostatic potential profiles of Fig.10 produces the parallel electric fields of Eq. (30), which are shown in Fig. 11. These fields are generally small in the SOL but become quite large in the divertors, particularly in the vicinity of the target plates.

As discussed in connection with Eq. (34), the implication of Eq. (19) is that the radial gradient of the electrostatic potential (the radial electric field) should be approximately proportional to the radial temperature gradient, which is characterized by the parameter $\Delta_T^{-1} = -dT/Tdr$. Using $\Delta_T = 2$ cm and the temperature profiles of Fig. 8, Eq. (34) yields the radial electric fields shown in Fig. 12. These radial electric fields are quite different with and without drifts and for the B(-) and B(+) toroidal field directions, primarily because of the difference caused in the electrostatic potentials of Fig. 10 by the differences in parallel current distributions shown in Fig. 9. For the B(-/+) field direction, the positive/negative radial electric field in the SOL corresponds to the temperature decreasing radially outward from the separatrix. In the divertor, the experimental evidence is that the peak in the temperature profile just in front of the target is somewhat outside the separatrix, so that at the separatrix there is a transition from a ‘negative’ temperature gradient in the SOL to a positive temperature gradient at the target plate, leading to an oppositely directed radial electric field into the private flux region.

Parallel flows

In the absence of drifts, because of the symmetry of the geometry and of the particle source from the core plasma into the SOL, the particle flows go symmetrically to the inner and outer divertor targets, as shown for D in Fig. 13. The sputtered particle sources in front of the divertor targets for C are also symmetric, and the resulting C particle fluxes are symmetric in the absence of drifts, as shown in Fig. 14. For D, the principle source of ions is the particle flux Γ_{\perp}^{sep} from the core, although there is a smaller source due to ionization of neutrals (primarily in the divertor). Without drifts, flow stagnation is at the symmetry point (between regions 25 and 26) at the crown of the SOL, as shown for in Fig. 13. For C the source is the sputtered carbon from the divertor plates deposited uniformly in the first two regions (1 and 2, 50 and 49), which is basically entrained in the high deuterium flow towards the plates in these regions.

Turning the drifts on produces two types of effects. First, the parallel ExB and grad-B drifts of Eqs. (36) and (26) produce a local increase or decrease in particle parallel flow velocity. Second, the outward and inward radial particle drifts of Eqs. (24), (30) and (37) produce sources and sinks of particles in the SOL and divertor, which affect the parallel particle flux as indicated by Eqs. (38) and (50). The parallel deuterium ion flux must increase or decrease in response to

this variation in ion sources and sinks to satisfy the continuity equation. The momentum balance equation is dominated by the pressure term in the SOL, which produces the relatively flat ion distribution over the SOL, so the variation in ion flux requires the variation in deuterium parallel velocity shown in Fig. 13.

With reference to Fig.5 for the B(-) field direction, both the grad-B and ExB radial drifts are out of the core, providing a particle source in the SOL between the X-point (region 10) and the mid-plane (region 18) of the inner SOL. Between the mid-plane (region 18) and the crown (region 25) the grad-B drift is inward and the ExB drift is outward, providing a sink and a source of particles to the SOL. Between the crown (region 26) and the mid-plane (region 33) of the outer divertor both drifts are inward from the SOL into the core, providing a particle sink in the SOL. From the mid-plane (region 33) to the X-point (region 41) the grad-B drift is outward and the ExB drift is inward, providing a source and a sink, respectively, of particles to the SOL. The diamagnetic drift is relatively smaller in the SOL. The particle flux variation in the SOL for deuterium for the B(-) field direction shown in Fig 13 reflects this variation in particle source and sink distributions. Note that there are three stagnation points in the deuterium parallel flow in the SOL for the B(-) drifts. Recent probe measurements of deuterium flow in a DIII-D L-mode discharge with the same B(-) field direction found a similar magnitude of deuterium flow in the crown region and also two flow stagnation points²⁰. When the field direction is changed from B(-) to B(+) all of the radial drift directions are reversed, reversing the particle source and sink distributions in the SOL and resulting in the deuterium velocity shown in Fig. 13

The calculated carbon parallel flow distributions are shown in Fig. 14. The same type of variation in particle sources and sinks because of the radial drifts also is present for carbon, but obviously other factors are dominant in the carbon force balance because the carbon parallel flows are of the opposite sign from the deuterium parallel flows in many locations.

Penetration of injected argon into the core plasma

It has been observed experimentally²¹ in DIII-D H-mode discharges that the penetration of the core plasma by argon injected into the private flux region of the divertor is significantly greater when the ion grad-B drift is towards the divertor [B(-)] than away from the divertor [B(+)]. In the model of this paper, the net penetration of argon from the SOL into the core can

be characterized by the parameter $\int_{\xi^{Xin}}^{\xi^{Xout}} n_{Ar} \left(v_{E_{\parallel}XB,Ar}^r + v_{B,Ar}^r + v_{dia,Ar}^r \right) d\xi < 0$, indicating a net radially

inward (-) drift. This parameter is calculated to be < 0 for the B (-) field direction shown in the Figs. 1-4, with the ion grad-B drift direction into the divertor, and to be > 0 for the reversed B(+) field direction with the ion grad-B drift direction out of the divertor, in qualitative agreement with the experimental observation. The significantly lower argon density shown in the divertor and SOL in Fig. 7 for the B(-) than the B(+) magnetic field configurations is also indicative of this same trend; since both calculations were performed with the same argon source and recycling coefficient, the lower argon concentration in the SOL for B(-) than for B(+) indicates a larger argon concentration in the core (by a factor 2-3).

IV. Summary

A computationally tractable model has been developed for the calculation of density, temperature, flow, current, and electrostatic potential and fields along the separatrix in tokamak scrape-off layers and divertors. The calculation is carried out in a 2D strip following the magnetic field lines around the tokamak from the inner to the outer divertor targets. Cross-field transport and magnetic geometry effects are treated analytically, reducing the calculation to a coupled set of nonlinear equations along the field lines, which are integrated numerically.

The calculation model was applied to calculate the effects of drifts and toroidal magnetic field direction on flows, currents, electric fields, density and temperature distributions in a model problem with parameters characteristic of a DIII-D H-mode discharge. A number of interesting phenomena—multiple reversal of parallel flows and currents in the SOL, reversal of the sign of the electrostatic potential and electric fields with the reversal of the toroidal magnetic field direction, larger penetration of the core plasma by argon injected in the divertor when the ion gradB drift was towards than away from the divertor, etc.—were predicted, some of which have been experimentally observed.

Acknowledgement

The author would like to express his appreciation to R. Isler, R. Groebner, M. Groth, T. Petrie, M. Schaeffer and G. Staebler for discussion of various aspects of this work and to General Atomics for hosting him during much of it. The work was supported by the U. S. Department of Energy Grant No. DE-FG02-00-ER54538 with the Georgia Tech Research Corporation.

References

1. P. C. Stangeby, *The Plasma Boundary of Magnetic Fusion Devices*, IOP Press, Bristol (2000).
2. K. Borrass, *Nucl. Fusion*, 31, 1035 (1991).
3. R. Maingi, M. A. Mahdavi, T. Jernigan, *et al.*, *Phys. Plasmas*, 4, 1752 (1997).
4. W. M. Stacey, *Phys. Plasmas*, 5, 1015 (1998).
5. G. M. Staebler, *Nucl. Fusion*, 36, 1437 (1996).
6. M. J. Schaffer, A. V. Chankin, H. Y. Guo, *et al.*, *Nucl. Fusion*, 37, 83 (1997).
7. G. J. Radford, *et al.*, *Contrib. Plasma Phys.*, 36, 187 (1996).
8. R. Zagorski, H. Gerhauser and H. A. Claassen, *Contrib. Plasma Phys.*, 38, 61 (1996).
9. T. D. Rognlien, D. D. Ryutov, N. Mattor and G. D. Porter, *Phys. Plasmas*, 5, 1851 (1999); *Contrib. Plasma Phys.*, 38, 152 (1998); *Plasma Phys. Control. Fusion*, 47, A283 (2005)
10. V. A. Rozhansky, S. P. Voskoboynikov, E. G. Kaveeva, D. P. Coster and R. Schneider, *Nucl. Fusion*, 41, 387 (2001); 42, 1110 (2002); 43, 614 (2003); *Contrib. Plasma Phys.*, 46, 575 (2006).
11. C. S. Chang and S. Ku, *Phys. Plasmas*, 15, 062510 (2008).
12. J. Luxon, *Nucl. Fusion*, 42, 6149 (2002).
13. M. J. Schaffer, B. D. Bray, J. A. Boedo, *et al.*, *Phys. Plasmas*, 8, 2118 (2001).
14. W. M. Stacey, *Nucl. Fusion*, 40, 965 (2000).
15. E. W. Thomas and W. M. Stacey, *Phys. Plasmas*, 4, 678 (1997); 2, 3740 (1995).
16. M. Keilhacker, R. Simonini, A. Taroni and M. L. Watkins, *Nucl. Fusion*, 31, 535 (1991).
17. W. M. Stacey, *Fusion Plasma Physics*, Wiley-VCH, Weinheim (2005), ch 13.
18. G. D. Porter, S. L. Allen, M. Brown, *et al.*, *Phys. Plasmas*, 3, 1967 (1996).
19. M. J. Shaeffer, General Atomics, private communication (2008).
20. M. Groth, G. D. Porter, J. A. Boedo, *et al.*, "Measurements and simulations of main scrape-off layer flows in DIII-D", *Plasma Surface Interaction Conf.* (Toledo, 2008), *J. Nucl. Mater.* (to be published).
21. T. W. Petrie, N. H. Brooks, M. E. Fenstermacher, *et al.*, *Nucl. Fusion*, 48, (2008); also *Plasma Surface Interaction Conf.* (Toledo, 2008), *J. Nucl. Mater.* (to be published).

List of Figures

- Figure 1. Geometric model of SOL-Divertor.
- Figure 2. Schematic illustration of direction of radial and parallel components of vertical (downward for B(-) toroidal magnetic field direction) grad-B and curvature drifts.
- Figure 3. Schematic of direction of parallel electrostatic field and associated radial ExB drifts for electrostatic potential increasing from divertor target to SOL crown and B(-) toroidal magnetic field direction.
- Figure 4. Schematic of direction of radial electrostatic field $E_r = -\partial\phi/\partial r \sim -\partial T_e/\partial r$ and corresponding parallel ExB drift in SOL (inward temperature gradient) and divertor (outward temperature gradient) for B(-) toroidal field direction.
- Figure 5. Radial ExB, gradB and diamagnetic drift velocities for deuterium ions. B(-) toroidal magnetic field direction.
- Figure 6. Parallel gradB and ExB drift particle fluxes for deuterium. B(-) toroidal magnetic field direction.
- Figure 7. Deuterium, carbon and argon ion densities in divertor (locations 1-9 and 42-50).
- Figure 8. Temperature distribution in divertor (regions 1-9 and 42-50) and SOL.
- Figure 9. Parallel plasma current density in divertor (regions 1-9 and 42-50) and SOL.
- Figure 10. Electrostatic potential distribution in divertor (regions 1-9 and 42-50) and SOL.
- Figure 11. Parallel electrostatic field distribution in divertor (regions 1-9 and 42-50) and SOL.
- Figure 12. Radial electrostatic field distribution in divertor (regions 1-9 and 42-50) and SOL.
- Figure 13. Parallel deuterium ion velocity in divertor (regions 1-9 and 42-50) and SOL.
- Figure 14. Parallel carbon ion velocity in divertor (regions 1-9 and 42-50) and SOL.

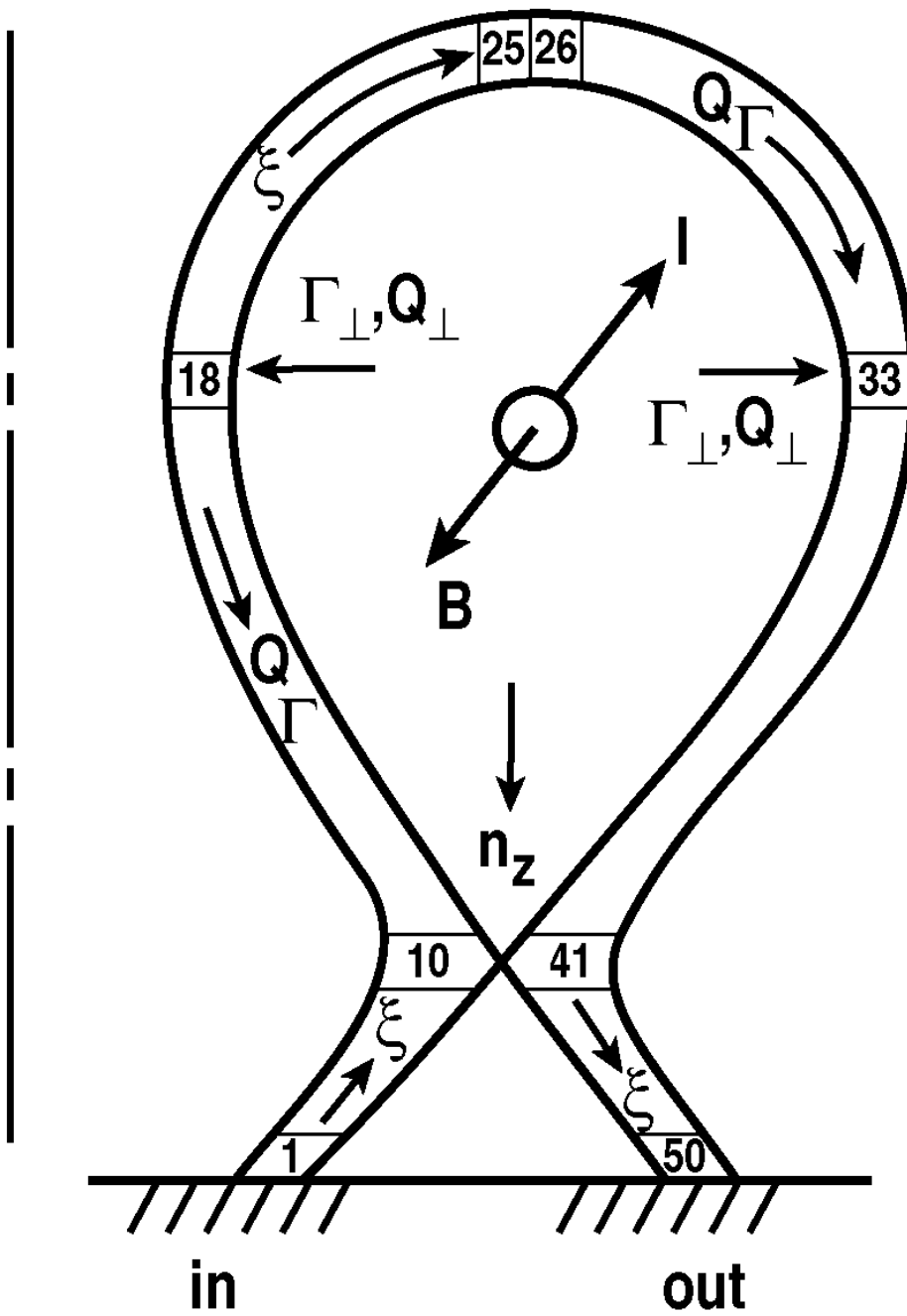


Figure 1. Geometric model of SOL-Divertor.

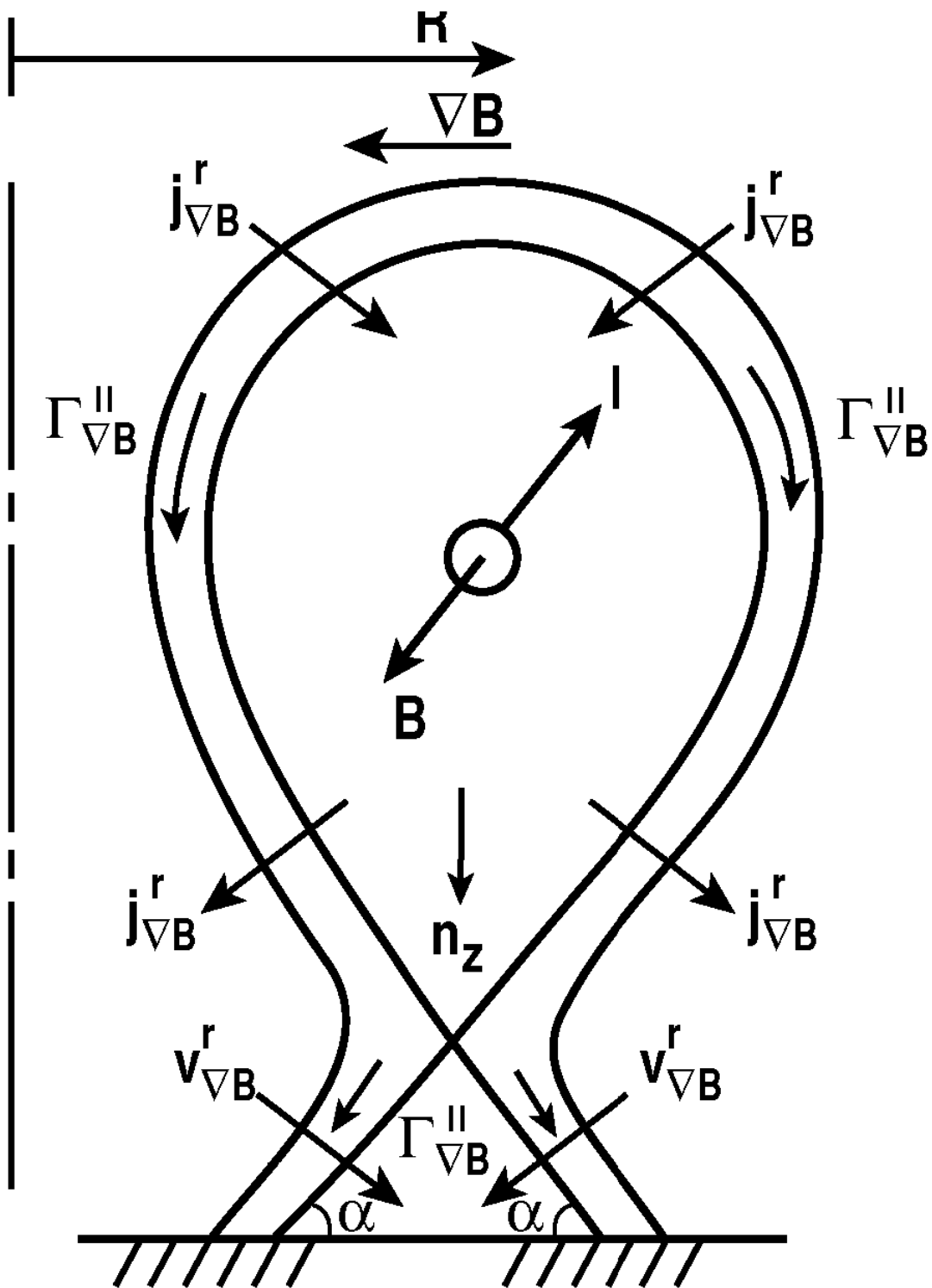


Figure 2 Schematic illustration of direction of radial and parallel components of vertical (downward for B(-) toroidal magnetic field direction) grad-B and curvature drifts.

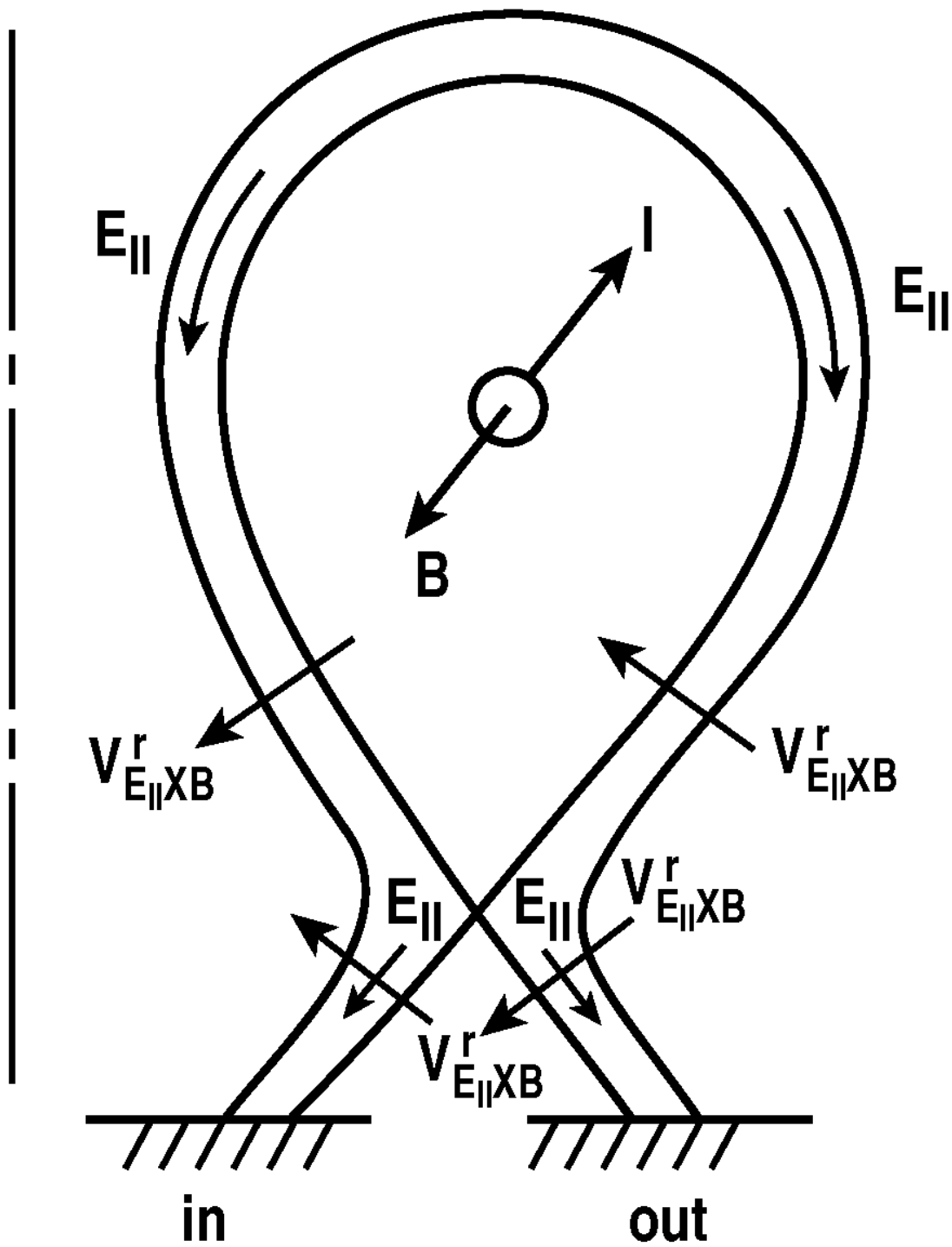


Figure 3 Schematic of direction of parallel electrostatic field and associated radial ExB drifts for electrostatic potential increasing from divertor target to SOL crown and B(-) toroidal magnetic field direction.

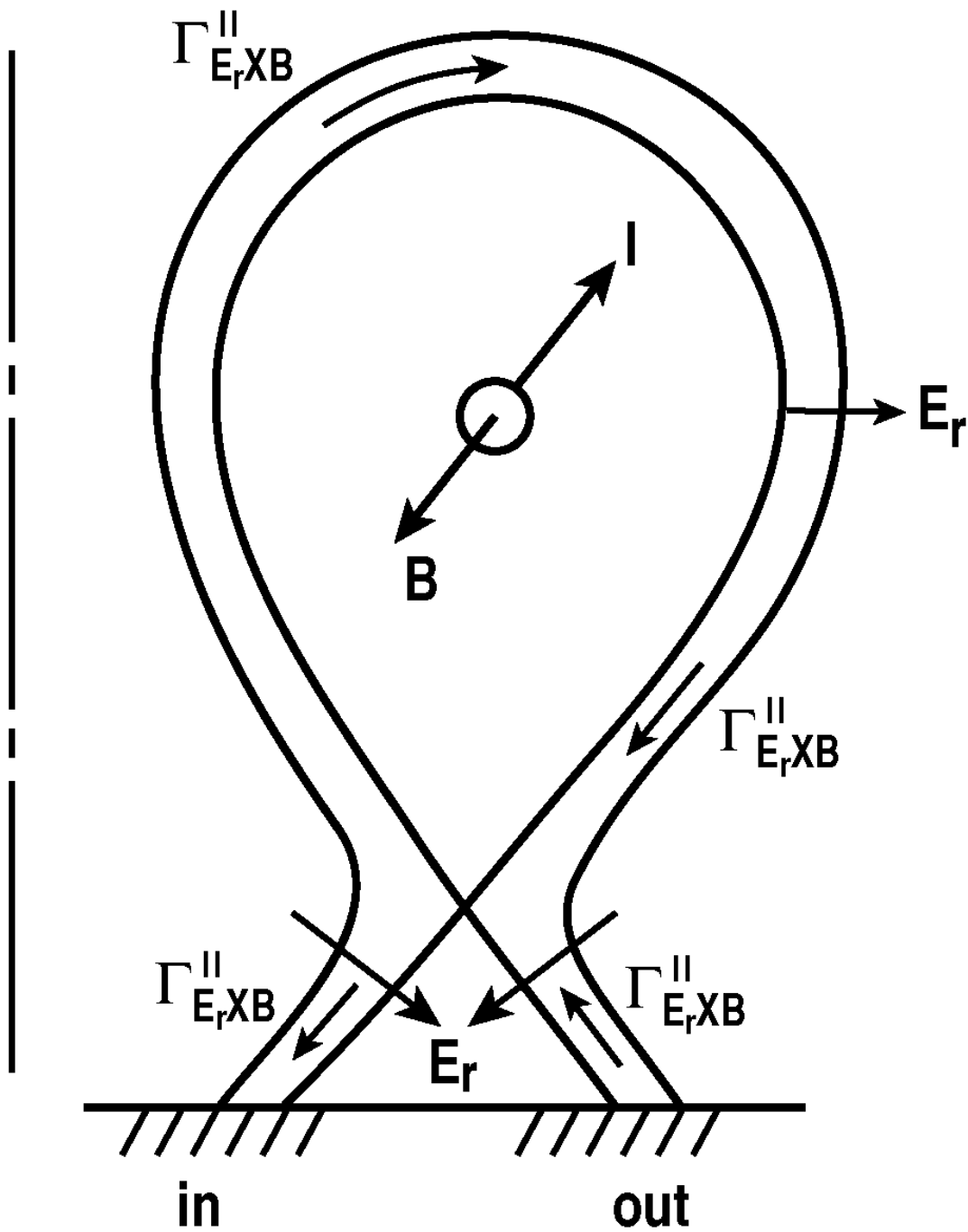


Figure 4 Schematic of direction of radial electrostatic field $E_r = -\partial\phi/\partial r \sim -\partial T_e/\partial r$ and corresponding parallel $E \times B$ drift in SOL (inward temperature gradient) and divertor (outward temperature gradient) for B(-) toroidal field direction.

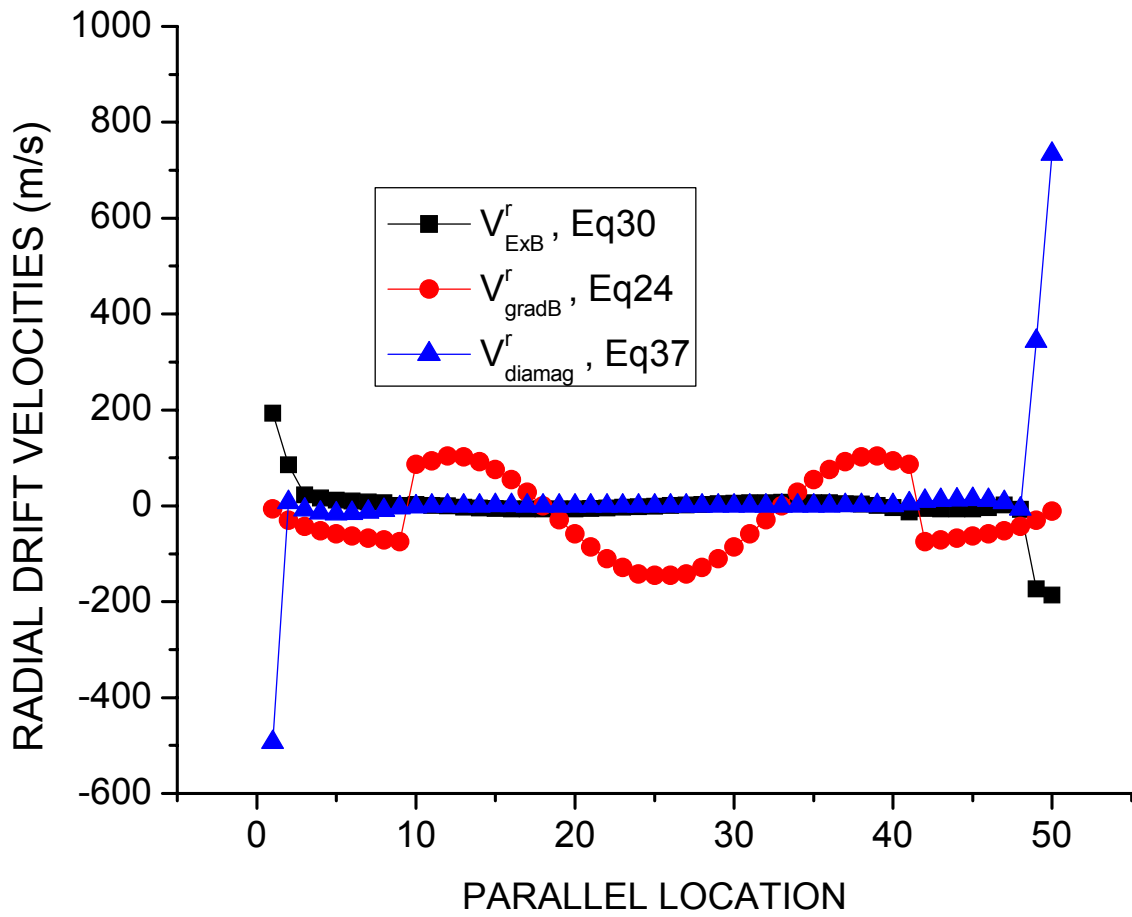


fig 5

Figure 5 Radial ExB, gradB and diamagnetic drift velocities for deuterium ions. B(-) toroidal magnetic field direction.

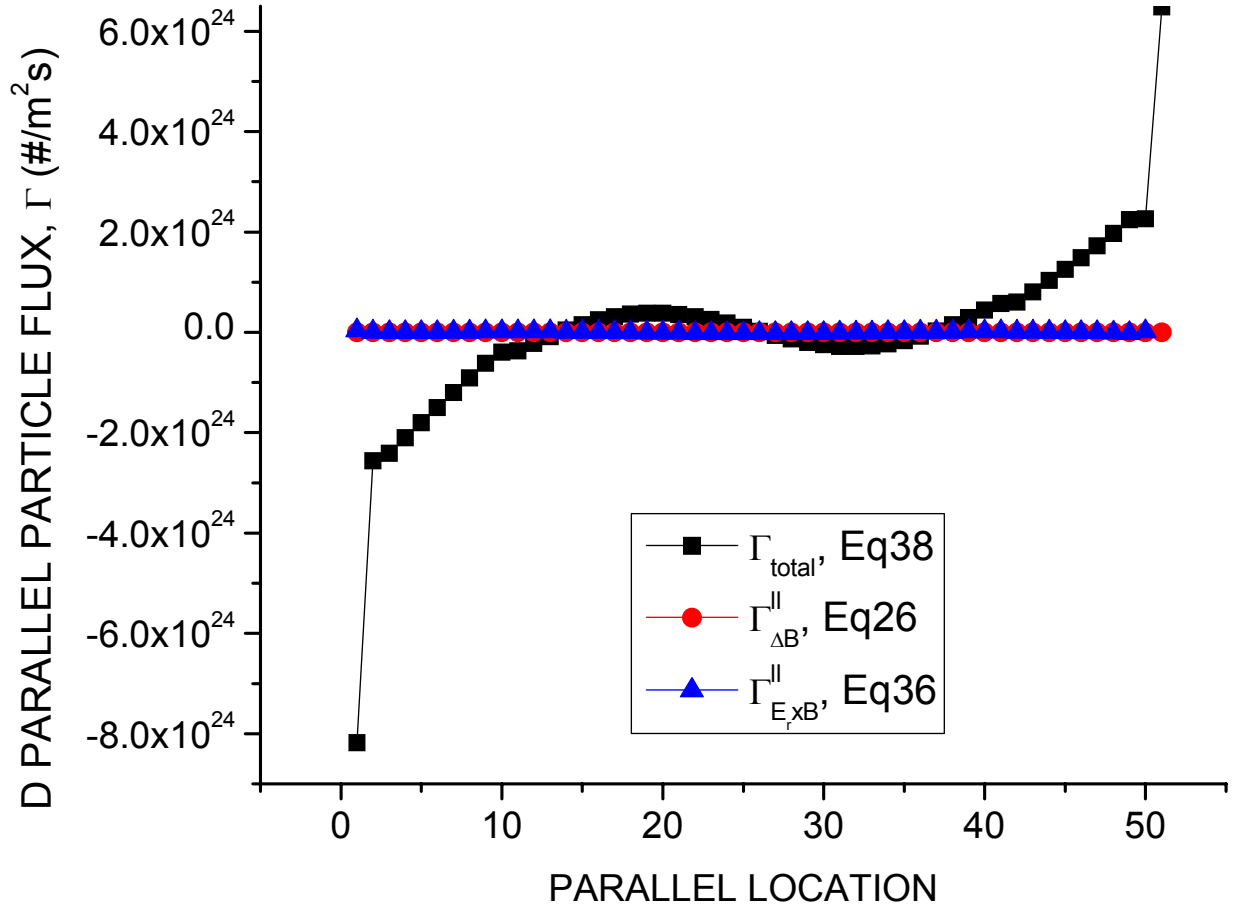


fig 6

Figure 6 Parallel gradB and ExB drift particle fluxes for deuterium. B(-) toroidal magnetic field direction.

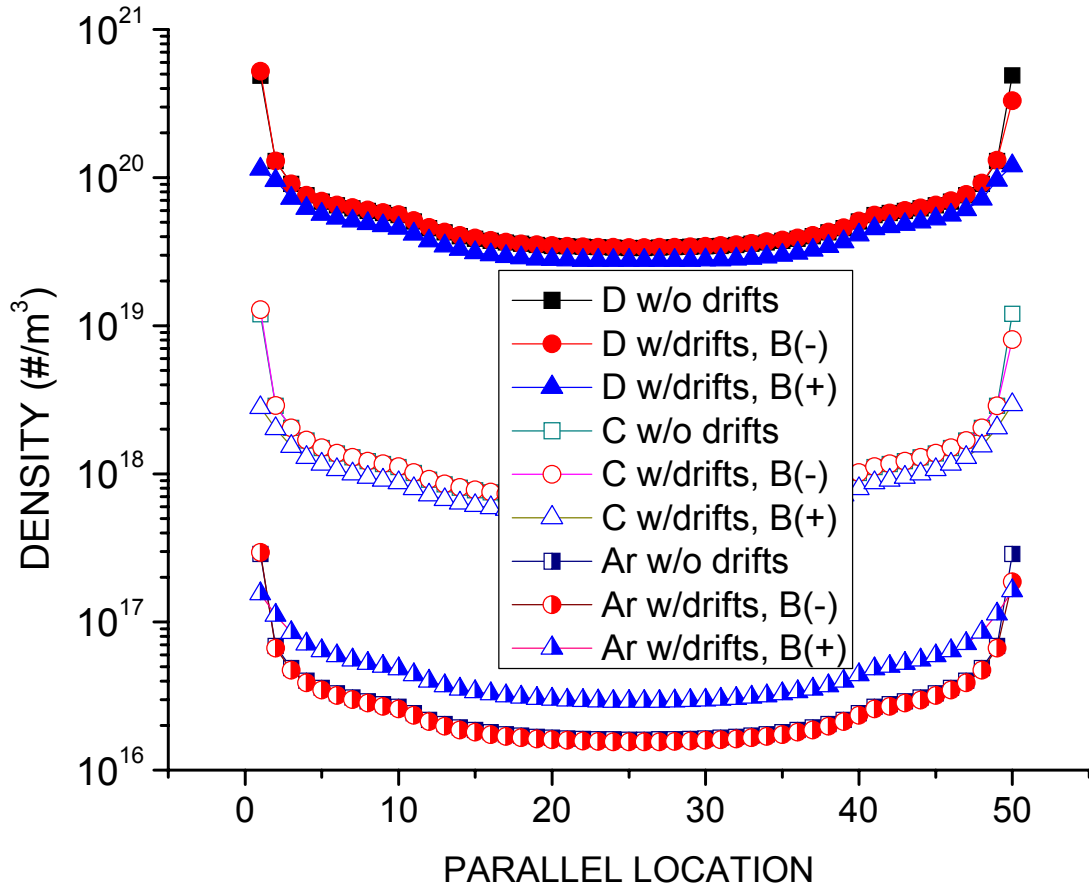


fig 7

Figure 7 Deuterium, carbon and argon ion densities in divertor (locations 1-9 and 42-50).

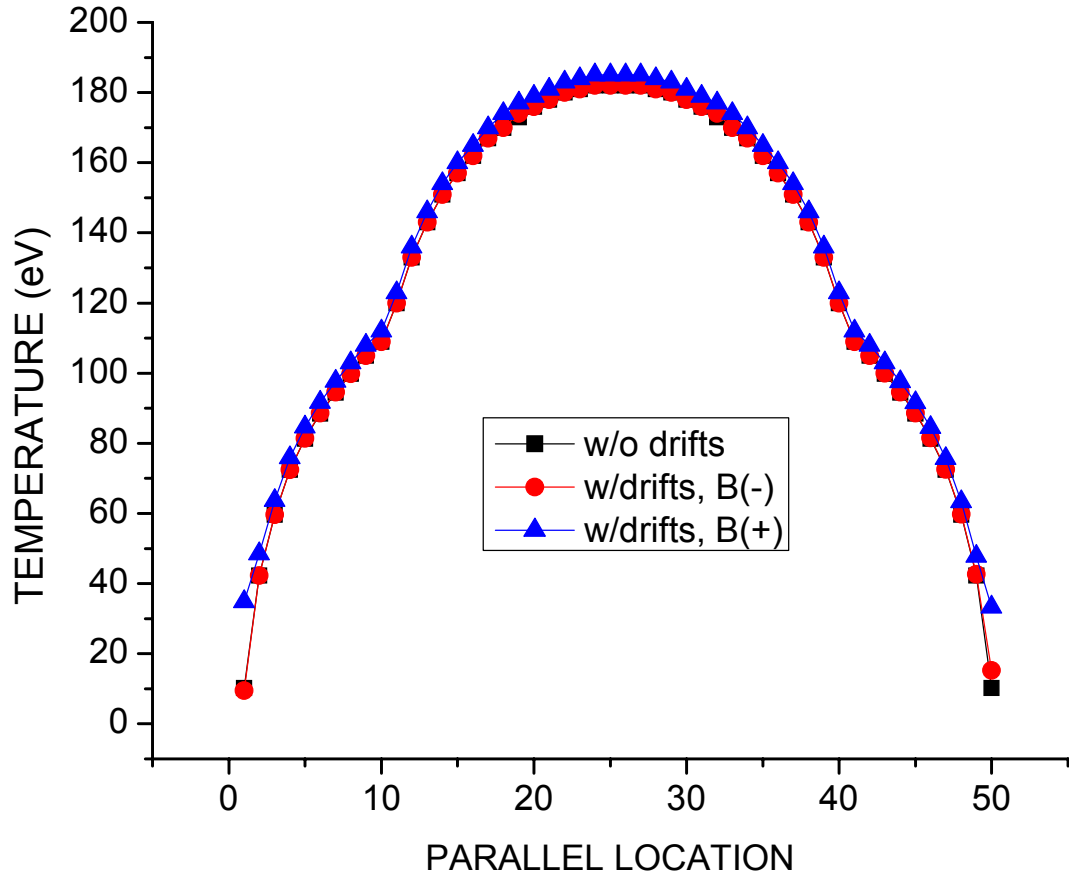


fig 8

Figure 8 Temperature distribution in divertor (regions 1-9 and 42-50) and SOL.

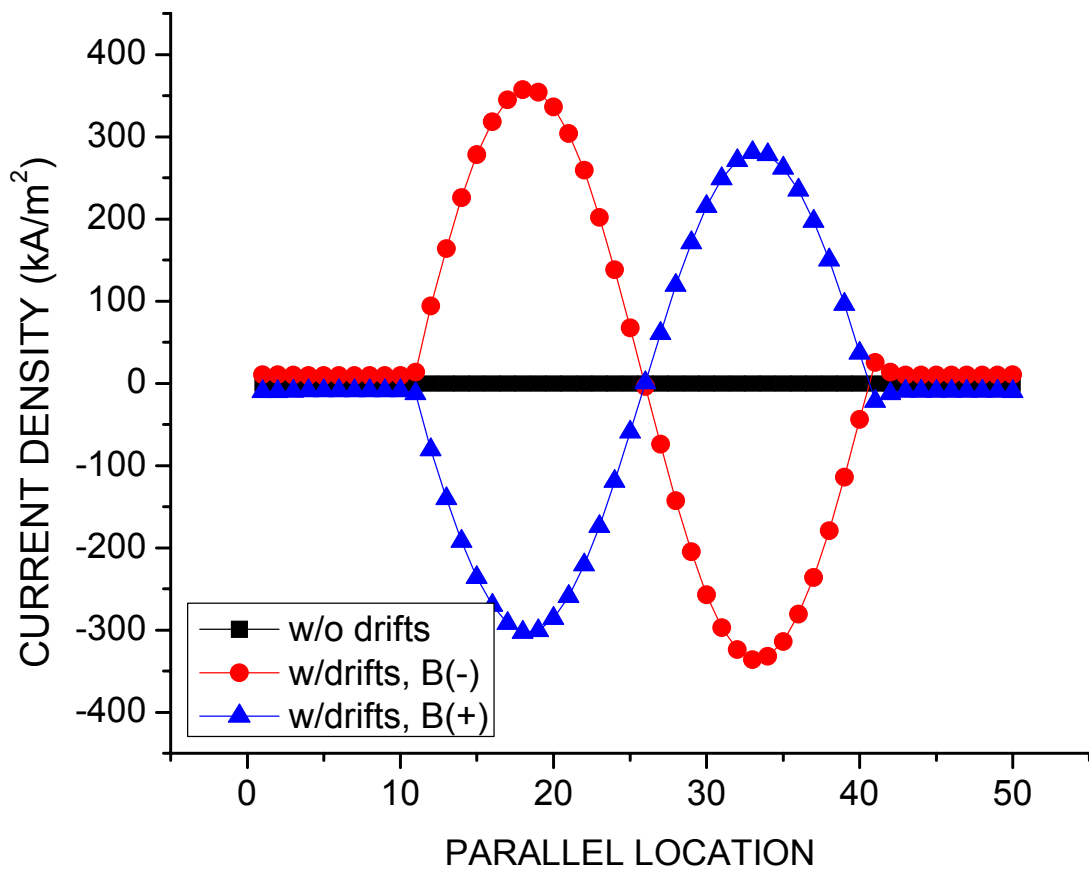


fig 9

Figure 9 Parallel plasma current density in divertor (regions 1-9 and 42-50) and SOL.

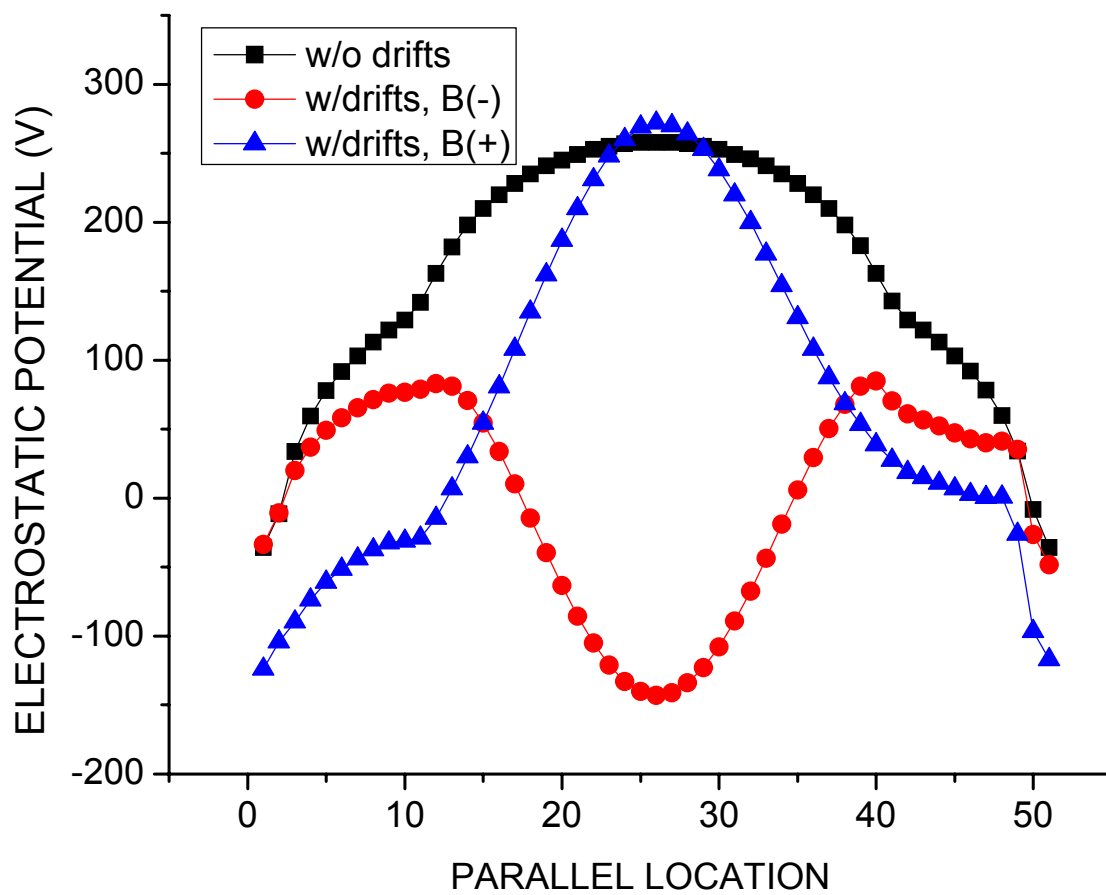


fig 10

Figure 10 Electrostatic potential distribution in divertor (regions 1-9 and 42-50) and SOL.

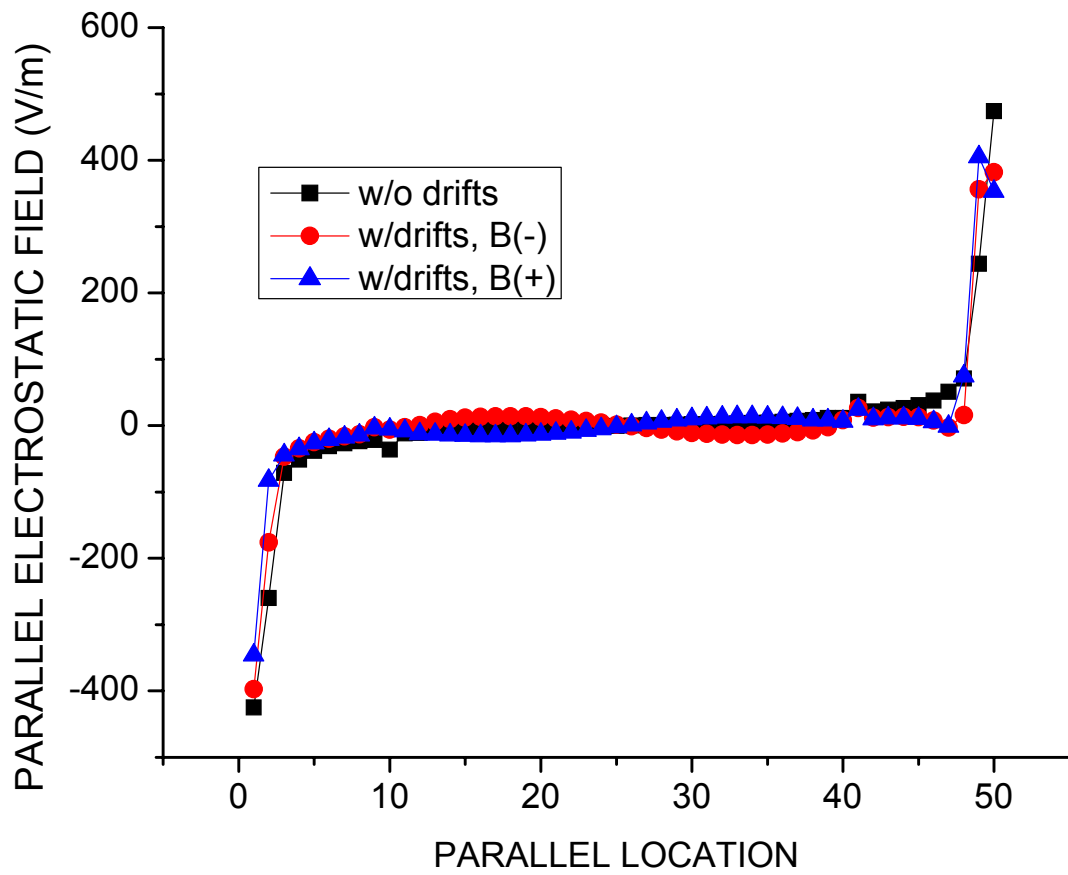


fig 11

Figure 11 Parallel electrostatic field distribution in divertor (regions 1-9 and 42-50) and SOL.

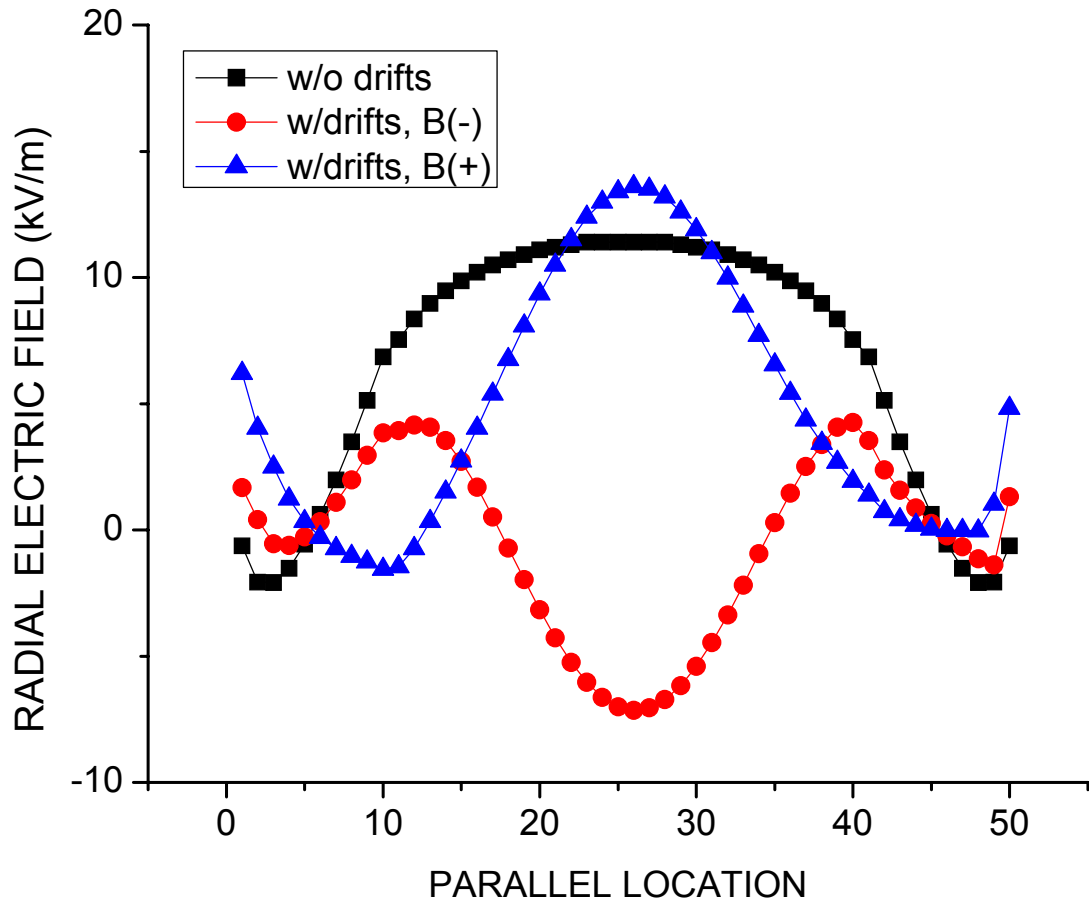


fig 12

Figure 12 Radial electrostatic field distribution in divertor (regions 1-9 and 42-50) and SOL.

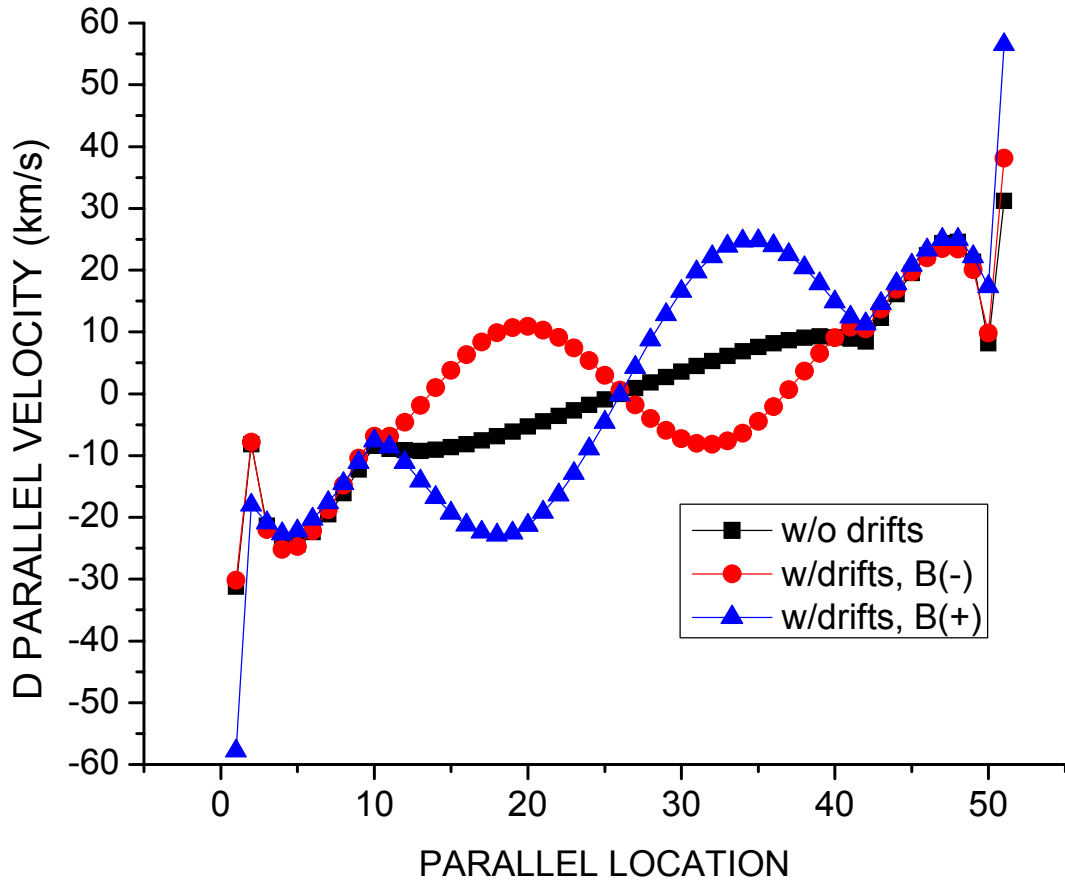


fig 13

Figure 13 Parallel deuterium ion velocity in divertor (regions 1-9 and 42-50) and SOL.

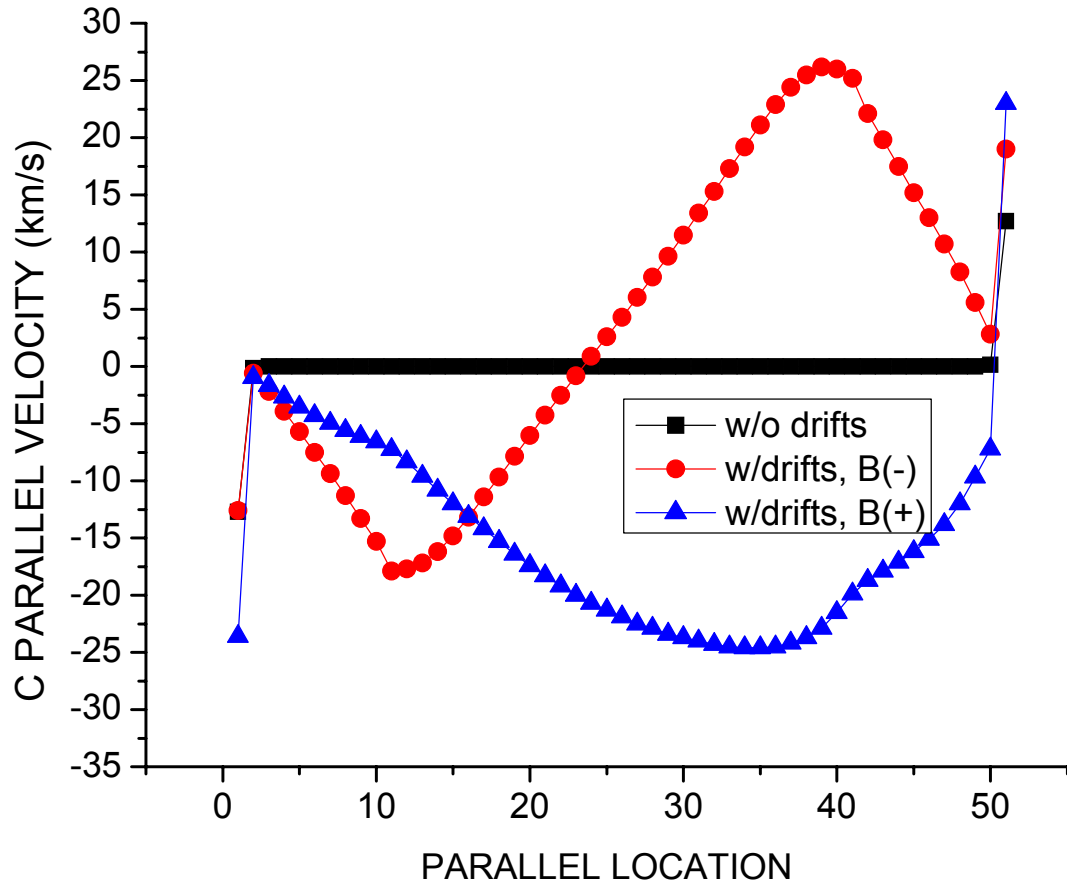


fig 14

Figure 14 Parallel carbon ion velocity in divertor (regions 1-9 and 42-50) and SOL.